

Fractal and Multifractal Time Series

Jan W. Kantelhardt
 Institute of Physics, Martin-Luther-University
 Halle-Wittenberg, 06099 Halle, Germany

November 26, 2024

Contents

1	Definition of the Subject and Its Importance	4
2	Introduction	4
3	Fractal and Multifractal Time Series	7
3.1	Fractality, Self-Affinity, and Scaling	7
3.2	Persistence, Long- and Short-term Correlations	8
3.3	Crossovers and Non-stationarities in Time Series	9
3.4	Multifractal Time Series	10
4	Methods for Stationary Fractal Time Series Analysis	11
4.1	Autocorrelation Function Analysis	11
4.2	Spectral Analysis	12
4.3	Hurst's Rescaled-Range Analysis	13
4.4	Fluctuation Analysis (FA)	14
5	Methods for Non-Stationary Fractal Time-Series Analysis	15
5.1	Wavelet Analysis	15
5.2	Discrete Wavelet Transform (WT) Approach	16
5.3	Detrended Fluctuation Analysis (DFA)	16
5.4	Detection of Trends and Crossovers with DFA	19
5.5	Sign and Magnitude (Volatility) DFA	21
5.6	Further Detrending Approaches	22
5.7	Centered Moving Average (CMA) Analysis	25

6	Methods for Multifractal Time Series Analysis	26
6.1	The Structure Function Approach and Singularity Spectra . . .	26
6.2	Wavelet Transform Modulus Maxima (WTMM) Method . . .	28
6.3	Multifractal Detrended Fluctuation Analysis (MF-DFA) . . .	29
6.4	Comparison of WTMM and MF-DFA	32
7	Statistics of Extreme Events in Fractal Time Series	33
7.1	Return Intervals Between Extreme Events	33
7.2	Distribution of Extreme Events	34
8	Simple Models for Fractal and Multifractal Time Series	36
8.1	Fourier Filtering	36
8.2	The Schmitz-Schreiber Method	37
8.3	The Extended Binomial Multifractal Model	38
8.4	The Bi-fractal Model	39
9	Future Directions	40
10	Bibliography	41

Glossary

- **Time series:** One dimensional array of numbers (x_i) , $i = 1, \dots, N$, representing values of an observable x usually measured equidistant (or nearly equidistant) in time.
- **Complex system:** A system consisting of many non-linearly interacting components. It cannot be split into simpler sub-systems without tampering the dynamical properties.
- **Scaling law:** A power law with a scaling exponent (e. g. α) describing the behaviour of a quantity F (e. g., fluctuation, spectral power) as function of a scale parameter s (e. g., time scale, frequency) at least asymptotically: $F(s) \sim s^\alpha$. The power law should be valid for a large range of s values, e. g., at least for one order of magnitude.
- **Fractal system:** A system characterised by a scaling law with a fractal, i. e., non-integer exponent. Fractal systems are characterised by self-similarity, i. e., a magnification of a small part is statistically equivalent to the whole.

- **Self-affine system:** Generalization of a fractal system, where different magnifications s and $s' = s^H$ have to be used for different directions in order to obtain a statistically equivalent magnification. The exponent H is called Hurst exponent. Self-affine time series and time series becoming self-affine upon integration are commonly denoted as fractal using a less strict terminology.
- **Multifractal system:** A system characterised by scaling laws with an infinite number of different fractal exponents. The scaling laws must be valid for the same range of the scale parameter.
- **Crossover:** Change point in a scaling law, where one scaling exponent applies for small scale parameters and another scaling exponent applies for large scale parameters. The center of the crossover is denoted by its characteristic scale parameter s_\times in this article.
- **Persistence:** In a persistent time series, a large value is usually (i. e., with high statistical preference) followed by a large value and a small value is followed by a small value. A fractal scaling law holds at least for a limited range of scales.
- **Short-term correlations:** Correlations that decay sufficiently fast that they can be described by a characteristic correlation time scale; e. g., exponentially decaying correlations. A crossover to uncorrelated behaviour is observed on larger scales.
- **Long-term correlations:** Correlations that decay sufficiently slow that a characteristic correlation time scale cannot be defined; e. g., power-law correlations with an exponent between 0 and 1. Power-law scaling is observed on large time scales and asymptotically. The term long-range correlations should be used if the data is not a time series.
- **Non-stationarities:** If the mean or the standard deviation of the data values change with time, the weak definition of stationarity is violated. The strong definition of stationarity requires that all moments remain constant, i. e., the distribution density of the values does not change with time. Non-stationarities like monotonous, periodic, or step-like trends are often caused by external effects. In a more general sense, changes in the dynamics of the system also represent non-stationarities.

1 Definition of the Subject and Its Importance

Data series generated by complex systems exhibit fluctuations on a wide range of time scales and/or broad distributions of the values. In both equilibrium and non-equilibrium situations, the natural fluctuations are often found to follow a scaling relation over several orders of magnitude. Such scaling laws allow for a characterisation of the data and the generating complex system by fractal (or multifractal) scaling exponents, which can serve as characteristic fingerprints of the systems in comparisons with other systems and with models. Fractal scaling behaviour has been observed, e. g., in many data series from experimental physics, geophysics, medicine, physiology, and even social sciences. Although the underlying causes of the observed fractal scaling are often not known in detail, the fractal or multifractal characterisation can be used for generating surrogate (test) data, modelling the time series, and deriving predictions regarding extreme events or future behaviour. The main application, however, is still the characterisation of different states or phases of the complex system based on the observed scaling behaviour. For example, the health status and different physiological states of the human cardiovascular system are represented by the fractal scaling behaviour of the time series of intervals between successive heartbeats, and the coarsening dynamics in metal alloys are represented by the fractal scaling of the time-dependent speckle intensities observed in coherent X-ray spectroscopy.

In order to observe fractal and multifractal scaling behaviour in time series, several tools have been developed. Besides older techniques assuming stationary data, there are more recently established methods differentiating truly fractal dynamics from fake scaling behaviour caused by non-stationarities in the data. In addition, short-term and long-term correlations have to be clearly distinguished to show fractal scaling behaviour unambiguously. This article describes several methods originating from Statistical Physics and Applied Mathematics, which have been used for fractal and multifractal time series analysis in stationary and non-stationary data.

2 Introduction

The characterisation and understanding of complex systems is a difficult task, since they cannot be split into simpler subsystems without tampering the dynamical properties. One approach in studying such systems is the recording of long *time series* of several selected variables (observables), which reflect the state of the system in a dimensionally reduced representation. Some

systems are characterised by periodic or nearly periodic behaviour, which might be caused by oscillatory components or closed-loop regulation chains. However, in truly complex systems such periodic components are usually not limited to one or two characteristic frequencies or frequency bands. They rather extend over a wide spectrum, and fluctuations on many time scales as well as broad distributions of the values are found. Often no specific lower frequency limit – or, equivalently, upper characteristic time scale – can be observed. In these cases, the dynamics can be characterised by *scaling laws* which are valid over a wide (possibly even unlimited) range of time scales or frequencies; at least over orders of magnitude. Such dynamics are usually denoted as *fractal* or *multifractal*, depending on the question if they are characterised by one scaling exponent or by a multitude of scaling exponents.

The first scientist who applied fractal analysis to natural time series is Benoit B. Mandelbrot [1, 2, 3], who included early approaches by H.E. Hurst regarding hydrological systems [4, 5]. For extensive introductions describing fractal scaling in complex systems, we refer to [6, 7, 8, 9, 10, 11, 12, 13]. In the last decade, fractal and multifractal scaling behaviour has been reported in many natural time series generated by complex systems, including

- geophysics time series (recordings of temperature, precipitation, water runoff, ozone levels, wind speed, seismic events, vegetational patterns, and climate dynamics),
- medical and physiological time series (recordings of heartbeat, respiration, blood pressure, blood flow, nerve spike intervals, human gait, glucose levels, and gene expression data),
- DNA sequences (they are not actually *time series*) ,
- astrophysical time series (X-ray light sources and sunspot numbers),
- technical time series (internet traffic, highway traffic, and neutronic power from a reactor),
- social time series (finance and economy, language characteristics, fatalities in conflicts), as well as
- physics data (also going beyond *time series*), e. g., surface roughness, chaotic spectra of atoms, and photon correlation spectroscopy recordings.

If one finds that a complex system is characterised by fractal (or multifractal) dynamics with particular scaling exponents, this finding will help in

obtaining predictions on the future behaviour of the system and on its reaction to external perturbations or changes in the boundary conditions. Phase transitions in the regulation behaviour of a complex system are often associated with changes in their fractal dynamics, allowing for a detection of such transitions (or the corresponding states) by fractal analysis. One example for a successful application of this approach is the human cardiovascular system, where the fractality of heartbeat interval time series was shown to reflect certain cardiac impairments as well as sleep stages [14, 15]. In addition, one can test and iteratively improve models of the system until they reproduce the observed scaling behaviour. One example for such an approach is climate modelling, where the models were shown to need input from volcanos and solar radiation in order to reproduce the long-term correlated (fractal) scaling behaviour [16] previously found in observational temperature data [17].

Fractal (or multifractal) scaling behaviour certainly cannot be assumed a priori, but has to be established. Hence, there is a need for refined analysis techniques, which help to differentiate truly fractal dynamics from fake scaling behaviour caused, e. g., by non-stationarities in the data. If conventional statistical methods are applied for the analysis of time series representing the dynamics of a complex system [18, 19], there are two major problems. (i) The number of data series and their durations (lengths) are usually very limited, making it difficult to extract significant information on the dynamics of the system in a reliable way. (ii) If the length of the data is extended using computer-based recording techniques or historical (proxy) data, non-stationarities in the signals tend to be superimposed upon the intrinsic fluctuation properties and measurement noise. Non-stationarities are caused by external or internal effects that lead to either continuous or sudden changes in the average values, standard deviations or regulation mechanism. They are a major problem for the characterisation of the dynamics, in particular for finding the scaling properties of given data.

Following the description of important properties of fractal and multifractal time series and the definition of our primary quantities of interest in Section 3, we focus on methods for the analysis of self-affine or (mono-)fractal data in Sections 4 and 5. While Section 4 describes traditional approaches for the analysis of stationary time series, Section 5 discusses more recently established methods applicable for non-stationary data. Section 6 describes techniques for multifractal time series analysis. The consequences of fractal scaling behaviour on the statistics of extreme events and their return intervals are presented in Section 7, and a few standard models for fractal and multifractal time series are described in Section 8 before an outlook on future directions in Section 9.

3 Fractal and Multifractal Time Series

3.1 Fractality, Self-Affinity, and Scaling

The topic of this article is the fractality (and/or multifractality) of time series. Since fractals and multifractals in general are discussed in many other articles of the encyclopedia, the concept is not thoroughly explained here. In particular, we refer to the articles ... and ... for the formalism describing fractal and multifractal structures, respectively.

In a strict sense, most time series are one dimensional, since the values of the considered observable are measured in homogeneous time intervals. Hence, unless there are missing values, the fractal dimension of the support is $D(0) = 1$. However, there are rare cases where most of the values of a time series are very small or even zero, causing a dimension $D(0) < 1$ of the support. In these cases, one has to be very careful in selecting appropriate analysis techniques, since many of the methods presented in this article are not accurate for such data; the Wavelet Transform Modulus Maxima technique (see Section 6.2) is the most advanced applicable method.

Even if the fractal dimension of support is one, the information dimension $D(1)$ and the correlation dimension $D(2)$ can be studied. As we will see in Section 6.1, $D(2)$ is in fact explicitly related to all exponents studied in monofractal time series analysis. However, usually a slightly different approach is employed based on the notion of self-affinity instead of (multi-)fractality. Here, one takes into account that the time axis and the axis of the measured values $x(t)$ are not equivalent. Hence, a rescaling of time t by a factor a may require rescaling of the series values $x(t)$ by a different factor a^H in order to obtain a statistically similar (i. e., self-similar) picture. In this case the scaling relation

$$x(t) \rightarrow a^H x(at) \tag{1}$$

holds for an arbitrary factor a , describing the data as self-affine (see, e. g., [6]). The *Hurst* exponent H (after the water engineer H.E. Hurst [4]) characterises the type of self affinity. Figure 1(a) shows several examples of self-affine time series with different H . The trace of a random walk (Brownian motion, third line in Fig. 1(a)), for example, is characterised by $H = 0.5$, implying that the position axis must be rescaled by a factor of 2 if the time axis is rescaled by a factor of 4. Note that self-affine series are often denoted as fractal even though they are not fractal in the strict sense. In this article the term "fractal" will be used in the more general sense including all data, where a Hurst exponent H can be reasonably defined.

The scaling behaviour of self-affine data can also be characterised by looking at their mean-square displacement. Since the mean-square displacement

of a random walker is known to increase linear in time, $\langle x^2(t) \rangle \sim t$, deviations from this law will indicate the presence of self-affine scaling. As we will see in Section 4.4, one can thus retrieve the Hurst (or self-affinity) exponent H by studying the scaling behaviour of the mean-square displacement, or the mean-square fluctuations $\langle x^2(t) \rangle \sim t^{2H}$.

3.2 Persistence, Long- and Short-term Correlations

Self-affine data are persistent in the sense that a large value is usually (i. e., with high statistical preference) followed by a large value and a small value is followed by a small value. For the trace of a random walk, persistence on all time scales is trivial, since a later position is just a former one plus some random increment(s). The persistence holds for all time scales, where the self-affinity relation (1) holds. However, the degree of persistence can also vary on different time scales. Weather is a typical example: while the weather tomorrow or in one week is probably similar to the weather today (due to a stable general weather condition), persistence is much harder to be seen on longer time scales.

Considering the increments $\Delta x_i = x_i - x_{i-1}$ of a self-affine series, (x_i) , $i = 1, \dots, N$ with N values measured equidistant in time, one finds that the Δx_i can be either persistent, independent, or anti-persistent. Examples for all cases are shown in Fig. 1(b). In our example of the random walk with $H = 0.5$ (third line in the figure), the increments (steps) are fully independent of each other. Persistent and anti-persistent increments, where a positive increment is likely to be followed by another positive or negative increment, respectively, are also leading to persistent integrated series $x_i = \sum_{j=1}^i \Delta x_j$.

For stationary data with constant mean and standard deviation the auto-covariance function of the increments,

$$C(s) = \langle \Delta x_i \Delta x_{i+s} \rangle = \frac{1}{N-s} \sum_{i=1}^{N-s} \Delta x_i \Delta x_{i+s}. \quad (2)$$

can be studied to determine the degree of persistence. If $C(s)$ is divided by the variance $\langle (\Delta x_i)^2 \rangle$, it becomes the auto-correlation function; both are identical if the data are normalised with unit variance. If the Δx_i are uncorrelated (as for the random walk), $C(s)$ is zero for $s > 0$. Short-range correlations of the increments Δx_i are usually described by $C(s)$ declining exponentially,

$$C(s) \sim \exp(-s/t_\times) \quad (3)$$

with a characteristic decay time t_\times . Such behaviour is typical for increments

generated by an auto-regressive (AR) process

$$\Delta x_i = c\Delta x_{i-1} + \varepsilon_i \quad (4)$$

with random uncorrelated offsets ε_i and $c = \exp(-1/t_\times)$. Figure 2(a) shows the auto-correlation function for one configuration of an AR process with $t_\times = 48$.

For so-called *long-range correlations* $\int_0^\infty C(s) ds$ diverges in the limit of infinitely long series ($N \rightarrow \infty$). In practice, this means that t_\times cannot be defined because it increases with increasing N . For example, $C(s)$ declines as a power-law

$$C(s) \propto s^{-\gamma} \quad (5)$$

with an exponent $0 < \gamma < 1$. Figure 2(b) shows $C(s)$ for one configuration with $\gamma = 0.4$. This type of behaviour can be modelled by the Fourier filtering technique (see Section 8.1). Long-term correlated, i. e. persistent, behaviour of the Δx_i leads to self-affine scaling behaviour of the x_i , characterised by $H = 1 - \gamma/2$, as will be shown below.

3.3 Crossovers and Non-stationarities in Time Series

Short-term correlated increments Δx_i characterised by a finite characteristic correlation decay time t_\times lead to a crossover in the scaling behaviour of the integrated series $x_i = \sum_{j=1}^i \Delta x_j$, see Fig. 2(a) for an example. Since the position of the crossover might be numerically different from t_\times , we denote it by s_\times here. Time series with a crossover are not self-affine and there is no unique Hurst exponent H characterising them. While $H > 0.5$ is observed on small time scales (indicating correlations in the increments), the asymptotic behaviour (for large time scales $s \gg t_\times$ and $\gg s_\times$) is always characterised by $H = 0.5$, since all correlations have decayed. Many natural recordings are characterised by pronounced short-term correlations in addition to scaling long-term correlations. For example, there are short-term correlations due to particular general weather situations in temperature data and due to respirational effects in heartbeat data. Crossovers in the scaling behaviour of complex time series can also be caused by different regulation mechanisms on fast and slow time scales. Fluctuations of river runoff, for example, show different scaling behaviour on time scales below and above approximately one year.

Non-stationarities can also cause crossovers in the scaling behaviour of data if they are not properly taken into account. In the most strict sense, non-stationarities are variations in the mean or the standard deviation of the data (violating weak stationarity) or the distribution of the data values

(violating strong stationarity). Non-stationarities like monotonous, periodic or step-like trends are often caused by external effects, e. g., by the greenhouse warming and seasonal variations for temperature records, different levels of activity in long-term physiological data, or unstable light sources in photon correlation spectroscopy. Another example for non-stationary data is a record consisting of segments with strong fluctuations alternating with segments with weak fluctuations. Such behaviour will cause a crossover in scaling at the time scale corresponding to the typical duration of the homogeneous segments. Different mechanisms of regulation during different time segments – like, e. g., different heartbeat regulation during different sleep stages at night – can also cause crossovers; they are regarded as non-stationarities here, too. Hence, if crossovers in the scaling behaviour of data are observed, more detailed studies are needed to find out the cause of the crossovers. One can try to obtain homogenous data by splitting the original series and employing methods that are at least insensitive to monotonous (polynomially shaped) trends.

To characterise a complex system based on time series, trends and fluctuations are usually studied separately (see, e. g., [20] for a discussion). Strong trends in data can lead to a false detection of long-range statistical persistence if only one (non-detrending) method is used or if the results are not carefully interpreted. Using several advanced techniques of scaling time series analysis (as described in Chapter 5) crossovers due to trends can be distinguished from crossovers due to different regulation mechanisms on fast and slow time scales. The techniques can thus assist in gaining insight into the scaling behaviour of the natural variability as well as into the kind of trends of the considered time series.

It has to be stressed that crossovers in scaling behaviour must not be confused with multifractality. Even though several scaling exponents are needed, they are not applicable for the same regime (i. e., the same range of time scales). Real multifractality, on the other hand, is characterised by different scaling behaviour of different moments over the full range of time scales (see next section).

3.4 Multifractal Time Series

Many records do not exhibit a simple monofractal scaling behaviour, which can be accounted for by a single scaling exponent. As discussed in the previous section, there might exist crossover (time-) scales s_{\times} separating regimes with different scaling exponents. In other cases, the scaling behaviour is more complicated, and different scaling exponents are required for different parts of the series. In even more complicated cases, such different scaling

behaviour can be observed for many interwoven fractal subsets of the time series. In this case a multitude of scaling exponents is required for a full description of the scaling behaviour in the same range of time scales, and a multifractal analysis must be applied.

Two general types of multifractality in time series can be distinguished: (i) Multifractality due to a broad probability distribution (density function) for the values of the time series, e. g. a Levy distribution. In this case the multifractality cannot be removed by shuffling the series. (ii) Multifractality due to different long-term correlations of the small and large fluctuations. In this case the probability density function of the values can be a regular distribution with finite moments, e. g., a Gaussian distribution. The corresponding shuffled series will exhibit non-multifractal scaling, since all long-range correlations are destroyed by the shuffling procedure. Randomly shuffling the order of the values in the time series is the easiest way of generating surrogate data; however, there are more advanced alternatives (see Chapter 8). If both kinds of multifractality are present, the shuffled series will show weaker multifractality than the original series.

A multifractal analysis of time series will also reveal higher order correlations. Multifractal scaling can be observed if, e. g., three or four-point correlations scale differently from the standard two-point correlations studied by classical autocorrelation analysis (Eq. (2)). In addition, multifractal scaling is observed if the scaling behaviour of small and large fluctuations is different. For example, extreme events might be more or less correlated than typical events.

4 Methods for Stationary Fractal Time Series Analysis

In this chapter we describe four traditional approaches for the fractal analysis of stationary time series, see [21, 22, 23] for comparative studies. The main focus is on the determination of the scaling exponents H or γ , defined in Eqs. (1) and (5), respectively, and linked by $H = 1 - \gamma/2$ in long-term persistent data. Methods taking non-stationarities into account will be discussed in the next chapter.

4.1 Autocorrelation Function Analysis

We consider a record (x_i) of $i = 1, \dots, N$ equidistant measurements. In most applications, the index i will correspond to the time of the measurements. We are interested in the correlation of the values x_i and x_{i+s} for different

time lags, i. e. correlations over different time scales s . In order to remove a constant offset in the data, the mean $\langle x \rangle = \frac{1}{N} \sum_{i=1}^N x_i$ is usually subtracted, $\tilde{x}_i \equiv x_i - \langle x \rangle$. Alternatively, the correlation properties of increments $\tilde{x}_i = \Delta x_i = x_i - x_{i-1}$ of the original series can be studied (see also Section 3.2). Quantitatively, correlations between \tilde{x} -values separated by s steps are defined by the (auto-) covariance function $C(s) = \langle \tilde{x}_i \tilde{x}_{i+s} \rangle$ or the (auto-) correlation function $C(s)/\langle \tilde{x}_i^2 \rangle$, see also Eq. (2).

As already mentioned in Section 3.2, the \tilde{x}_i are short-term correlated if $C(s)$ declines exponentially, $C(s) \sim \exp(-s/t_\times)$, and long-term correlated if $C(s)$ declines as a power-law $C(s) \propto s^{-\gamma}$ with a correlation exponent $0 < \gamma < 1$ (see Eqs. (3) and (5), respectively). As illustrated by the two examples shown in Fig. 2, a direct calculation of $C(s)$ is usually not appropriate due to noise superimposed on the data \tilde{x}_i and due to underlying non-stationarities of unknown origin. Non-stationarities make the definition of $C(s)$ problematic, because the average $\langle x \rangle$ is not well-defined. Furthermore, $C(s)$ strongly fluctuates around zero on large scales s (see Fig. 2(b)), making it impossible to find the correct correlation exponent γ . Thus, one has to determine the value of γ indirectly.

4.2 Spectral Analysis

If the time series is stationary, we can apply standard spectral analysis techniques (Fourier transform) and calculate the power spectrum $S(f)$ of the time series (\tilde{x}_i) as a function of the frequency f to determine self-affine scaling behaviour [24]. For long-term correlated data characterised by the correlation exponent γ , we have

$$S(f) \sim f^{-\beta} \quad \text{with} \quad \beta = 1 - \gamma. \quad (6)$$

The spectral exponent β and the correlation exponent γ can thus be obtained by fitting a power-law to a double logarithmic plot of the power spectrum $S(f)$. An example is shown in Fig. 3. The relation (6) can be derived from the Wiener-Khinchin theorem (see, e. g., [25]). If, instead of $\tilde{x}_i = \Delta x_i$ the integrated runoff time series is Fourier transformed, i. e., $\tilde{x}_i = x_i \sum_{j=1}^i \Delta x_j$, the resulting power spectrum scales as $S(f) \sim f^{-2-\beta}$.

Spectral analysis, however, does not yield more reliable results than auto-correlation analysis unless a logarithmic binning procedure is applied to the double logarithmic plot of $S(f)$ [21], see also Fig. 3. I. e., the average of $\log S(f)$ is calculated in successive, logarithmically wide bands from $a^n f_0$ to $a^{n+1} f_0$, where f_0 is the minimum frequency, $a > 1$ is a factor (e. g., $a = 1.1$), and the index n is counting the bins. Spectral analysis also requires stationarity of the data.

4.3 Hurst's Rescaled-Range Analysis

The first method for the analysis of long-term persistence in time series based on random walk theory has been proposed by the water construction engineer Harold Edwin Hurst (1880-1978), who developed it while working in Egypt. His so-called rescaled range analysis (R/S analysis) [1, 2, 4, 5, 6] begins with splitting of the time series (\tilde{x}_i) into non-overlapping segments ν of size (time scale) s (first step), yielding $N_s = \text{int}(N/s)$ segments altogether. In the second step, the *profile* (integrated data) is calculated in each segment $\nu = 0, \dots, N_s - 1$,

$$Y_\nu(j) = \sum_{i=1}^j (\tilde{x}_{\nu s+i} - \langle \tilde{x}_{\nu s+i} \rangle_s) = \sum_{i=1}^j \tilde{x}_{\nu s+i} - \frac{j}{s} \sum_{i=1}^s \tilde{x}_{\nu s+i}. \quad (7)$$

By the subtraction of the local averages, piecewise constant trends in the data are eliminated. In the third step, the differences between minimum and maximum value (*ranges*) $R_\nu(s)$ and the standard deviations $S_\nu(s)$ in each segment are calculated,

$$R_\nu(s) = \max_{j=1}^s Y_\nu(j) - \min_{j=1}^s Y_\nu(j), \quad S_\nu(s) = \sqrt{\frac{1}{s} \sum_{j=1}^s Y_\nu^2(j)}. \quad (8)$$

Finally, the rescaled range is averaged over all segments to obtain the fluctuation function $F(s)$,

$$F_{RS}(s) = \frac{1}{N_s} \sum_{\nu=0}^{N_s-1} \frac{R_\nu(s)}{S_\nu(s)} \sim s^H \quad \text{for } s \gg 1, \quad (9)$$

where H is the Hurst exponent already introduced in Eq. (1). One can show [1, 24] that H is related to β and γ by $2H \approx 1 + \beta = 2 - \gamma$ (see also Eqs. (6) and (14)). Note that $0 < \gamma < 1$, so that the right part of the equation does not hold unless $0.5 < H < 1$. The relationship does *not* hold in general for multifractal data. Note also that H actually characterises the self-affinity of the profile function (7), while β and γ refer to the original data.

The values of H , that can be obtained by Hurst's rescaled range analysis, are limited to $0 < H < 2$, and significant inaccuracies are to be expected close to the bounds. Since H can be increased or decreased by 1 if the data is integrated ($\tilde{x}_j \rightarrow \sum_{i=1}^j \tilde{x}_i$) or differentiated ($\tilde{x}_i \rightarrow \tilde{x}_i - \tilde{x}_{i-1}$), respectively, one can always find a way to calculate H by rescaled range analysis provided the data is stationary. While values $H < 1/2$ indicate long-term anti-correlated behaviour of the data \tilde{x}_i , $H > 1/2$ indicates long-term positively correlated behaviour. For power-law correlations decaying faster than $1/s$, we have $H = 1/2$ for large s values, like for uncorrelated data.

Compared with spectral analysis, Hurst's rescaled range analysis yields smoother curves with less effort (no binning procedure is necessary) and works also for data with piecewise constant trends.

4.4 Fluctuation Analysis (FA)

The standard fluctuation analysis (FA) [8, 26] is also based on random walk theory. For a time series (\tilde{x}_i) , $i = 1, \dots, N$, with zero mean, we consider the global profile, i. e., the cumulative sum (cf. Eq. (7))

$$Y(j) = \sum_{i=1}^j \tilde{x}_i, \quad j = 0, 1, 2, \dots, N, \quad (10)$$

and study how the fluctuations of the profile, in a given time window of size s , increase with s . The procedure is illustrated in Fig. 4 for two values of s . We can consider the profile $Y(j)$ as the position of a random walker on a linear chain after j steps. The random walker starts at the origin and performs, in the i th step, a jump of length \tilde{x}_i to the right, if \tilde{x}_i is positive, and to the left, if \tilde{x}_i is negative.

To find how the square-fluctuations of the profile scale with s , we first divide each record of N elements into $N_s = \text{int}(N/s)$ non-overlapping segments of size s starting from the beginning (see Fig. 4) and another N_s non-overlapping segments of size s starting from the end of the considered series. This way neither data at the end nor at the beginning of the record is neglected. Then we determine the fluctuations in each segment ν .

In the standard FA, we obtain the fluctuations just from the values of the profile at both endpoints of each segment $\nu = 0, \dots, N_s - 1$,

$$F_{\text{FA}}^2(\nu, s) = [Y(\nu s) - Y((\nu + 1)s)]^2, \quad (11)$$

(see Fig. 4) and analogous for $\nu = N_s, \dots, 2N_s - 1$,

$$F_{\text{FA}}^2(\nu, s) = [Y(N - (\nu - N_s)s) - Y(N - (\nu + 1 - N_s)s)]^2. \quad (12)$$

Then we average $F_{\text{FA}}^2(\nu, s)$ over all subsequences to obtain the mean fluctuation $F_2(s)$,

$$F_2(s) = \left[\frac{1}{2N_s} \sum_{\nu=0}^{2N_s-1} F_{\text{FA}}^2(\nu, s) \right]^{1/2} \sim s^\alpha. \quad (13)$$

By definition, $F_2(s)$ can be viewed as the root-mean-square displacement of the random walker on the chain, after s steps (the reason for the index 2 will become clear later). For uncorrelated x_i values, we obtain Fick's diffusion

law $F_2(s) \sim s^{1/2}$. For the relevant case of long-term correlations, where $C(s)$ follows the power-law behaviour of Eq. (5), $F_2(s)$ increases by a power law,

$$F_2(s) \sim s^\alpha \quad \text{with} \quad \alpha \approx H, \quad (14)$$

where the fluctuation exponent α is identical with the Hurst exponent H for mono-fractal data and related to γ and β by

$$2\alpha = 1 + \beta = 2 - \gamma. \quad (15)$$

The typical behaviour of $F_2(s)$ for short-term correlated and long-term correlated data is illustrated in Fig. 2. The relation (15) can be derived straightforwardly by inserting Eqs. (10), (2), and (5) into Eq. (11) and separating sums over products $\tilde{x}_i \tilde{x}_j$ with identical and different i and j , respectively.

The range of the α values that can be studied by standard FA is limited to $0 < \alpha < 1$, again with significant inaccuracies close to the bounds. Regarding integration or differentiation of the data, the same rules apply as listed for H in the previous section. The results of FA become statistically unreliable for scales s larger than one tenth of the length of the data, i. e. the analysis should be limited by $s < N/10$.

5 Methods for Non-Stationary Fractal Time-Series Analysis

5.1 Wavelet Analysis

The origins of wavelet analysis come from signal theory, where frequency decompositions of time series were studied [27, 28]. Like the Fourier transform, the wavelet transform of a signal $x(t)$ is a convolution integral to be replaced by a summation in case of a discrete time series $(\tilde{x}_i), i = 1, \dots, N$,

$$L_\psi(\tau, s) = \frac{1}{s} \int_{-\infty}^{\infty} x(t) \psi[(t - \tau)/s] dt = \frac{1}{s} \sum_{i=1}^N \tilde{x}_i \psi[(i - \tau)/s]. \quad (16)$$

Here, $\psi(t)$ is a so-called mother wavelet, from which all daughter wavelets $\psi_{\tau,s}(t) = \psi((t - \tau)/s)$ evolve by shifting and stretching of the time axis. The wavelet coefficients $L_\psi(\tau, s)$ thus depend on both, time position τ and scale s . Hence, the local frequency decomposition of the signal is described with a time resolution appropriate for the considered frequency $f = 1/s$ (i. e., inverse time scale).

All wavelets $\psi(t)$ must have zero mean. They are often chosen to be orthogonal to polynomial trends, so that the analysis method becomes insensitive to possible trends in the data. Simple examples are derivatives of a Gaussian, $\psi_{\text{Gauss}}^{(n)}(t) = \frac{d^n}{dt^n} \exp(-x^2/2)$, like the Mexican hat wavelet $-\psi_{\text{Gauss}}^{(2)}$ and the Haar wavelet, $\psi_{\text{Haar}}^{(0)}(t) = +1$ if $0 \leq t < 1$, -1 if $1 \leq t < 2$, and 0 otherwise. It is straightforward to construct Haar wavelet that are orthogonal to linear, quadratic and cubic trends, e. g., $\psi_{\text{Haar}}^{(1)}(t) = 1$ for $t \in [0, 1) \cup [2, 3)$, -2 for $t \in [1, 2)$, and 0 otherwise, or $\psi_{\text{Haar}}^{(2)}(t) = 1$ for $t \in [0, 1)$, -3 for $t \in [1, 2)$, $+3$ for $t \in [2, 3)$, -1 for $t \in [3, 4)$, and 0 otherwise.

5.2 Discrete Wavelet Transform (WT) Approach

A detrending fractal analysis of time series can be easily implemented by considering Haar wavelet coefficients of the profile $Y(j)$, Eq. (10) [29, 17]. In this case the convolution (16) corresponds to the addition and subtraction of mean values of $Y(j)$ within segments of size s . Hence, defining $\bar{Y}_\nu(s) = \frac{1}{s} \sum_{j=1}^s Y(\nu s + j)$, the coefficients can be written as

$$F_{\text{WT0}}(\nu, s) \equiv L_{\psi_{\text{Haar}}^{(0)}}(\nu s, s) = \bar{Y}_\nu(s) - \bar{Y}_{\nu+1}(s), \quad (17)$$

$$F_{\text{WT1}}(\nu, s) \equiv L_{\psi_{\text{Haar}}^{(1)}}(\nu s, s) = \bar{Y}_\nu(s) - 2\bar{Y}_{\nu+1}(s) + \bar{Y}_{\nu+2}(s), \quad \text{and} \quad (18)$$

$$F_{\text{WT2}}(\nu, s) \equiv L_{\psi_{\text{Haar}}^{(2)}}(\nu s, s) = \bar{Y}_\nu(s) - 3\bar{Y}_{\nu+1}(s) + 3\bar{Y}_{\nu+2}(s) - \bar{Y}_{\nu+3}(s) \quad (19)$$

for constant, linear and quadratic detrending, respectively. The generalization for higher orders of detrending is obvious. The resulting mean-square fluctuations $F_{\text{WT}n}^2(\nu, s)$ are averaged over all ν to obtain the mean fluctuation $F_2(s)$, see Eq. (13). Figure 5 shows typical results for WT analysis of long-term correlated, short-term correlated and uncorrelated data.

Regarding trend-elimination, wavelet transform WT0 corresponds to standard FA (see Section 4.4), and only constant trends in the profile are eliminated. WT1 is similar to Hurst's rescaled range analysis (see Section 4.3): linear trends in the profile and constant trends in the data are eliminated, and the range of the fluctuation exponent $\alpha \approx H$ is up to 2. In general, WT n determines the fluctuations from the n th derivative, this way eliminating trends described by $(n - 1)$ st-order polynomials in the data. The results become statistically unreliable for scales s larger than one tenth of the length of the data, just as for FA.

5.3 Detrended Fluctuation Analysis (DFA)

In the last 13 years *Detrended Fluctuation Analysis* (DFA), originally introduced by Peng et al. [30], has been established as an important method to

reliably detect long-range (auto-) correlations in non-stationary time series. The method is based on random walk theory and basically represents a linear detrending version of FA (see Section 4.4). DFA was later generalised for higher order detrending [15], separate analysis of sign and magnitude series [31] (see Section 5.5), multifractal analysis [32] (see Section 6.3), and data with more than one dimension [33]. Its features have been studied in many articles [34, 35, 36, 37, 38, 39]. In addition, several comparisons of DFA with other methods for stationary and non-stationary time-series analysis have been published, see, e. g., [21, 23, 40, 41] and in particular [22], where DFA is compared with many other established methods for short data sets, and [42], where it is compared with recently suggested improved methods. Altogether, there are about 450-500 papers applying DFA (till April 2008). In most cases positive auto-correlations were reported leaving only a few exceptions with anti-correlations, see, e. g., [43, 44, 45].

Like in the FA method, one first calculates the global profile according to Eq. (10) and divides the profile into $N_s = \text{int}(N/s)$ non-overlapping segments of size s starting from the beginning and another N_s segments starting from the end of the considered series. DFA explicitly deals with monotonous trends in a detrending procedure. This is done by estimating a polynomial trend $y_{\nu,s}^m(j)$ within each segment ν by least-square fitting and subtracting this trend from the original profile ('detrending'),

$$\tilde{Y}_s(j) = Y(j) - y_{\nu,s}^m(j). \quad (20)$$

The degree of the polynomial can be varied in order to eliminate constant ($m = 0$), linear ($m = 1$), quadratic ($m = 2$) or higher order trends of the profile function [15]. Conventionally the DFA is named after the order of the fitting polynomial (DFA0, DFA1, DFA2, ...). In DFA m , trends of order m in the profile $Y(j)$ and of order $m - 1$ in the original record \tilde{x}_i are eliminated. The variance of the detrended profile $\tilde{Y}_s(j)$ in each segment ν yields the mean-square fluctuations,

$$F_{\text{DFA}m}^2(\nu, s) = \frac{1}{s} \sum_{j=1}^s \tilde{Y}_s^2(j). \quad (21)$$

As for FA and discrete wavelet analysis, the $F_{\text{DFA}m}^2(\nu, s)$ are averaged over all segments ν to obtain the mean fluctuations $F_2(s)$, see Eq. (14). Calculating $F_2(s)$ for many s , the fluctuation scaling exponent α can be determined just as with FA. Figure 6 shows typical results for DFA of the same long-term correlated, short-term correlated and uncorrelated data studied already in Fig. 5.

We note that in studies that include averaging over many records (or one record cut into many separate pieces by the elimination of some unreliable intermediate data points) the averaging procedure (13) must be performed for all data. Taking the square root is always the final step after all averaging is finished. It is not appropriate to calculate $F_2(s)$ for parts of the data and then average the $F_2(s)$ values, since such a procedure will bias the results towards smaller scaling exponents on large time scales.

If $F_2(s)$ increases for increasing s by $F_2(s) \sim s^\alpha$ with $0.5 < \alpha < 1$, one finds that the scaling exponent $\alpha \approx H$ is related to the correlation exponent γ by $\alpha = 1 - \gamma/2$ (see Eq. (15)). A value of $\alpha = 0.5$ thus indicates that there are no (or only short-range) correlations. If $\alpha > 0.5$ for all scales s , the data are long-term correlated. The higher α , the stronger the correlations in the signal are. $\alpha > 1$ indicates a non-stationary local average of the data; in this case, FA fails and yields only $\alpha = 1$. The case $\alpha < 0.5$ corresponds to long-term anti-correlations, meaning that large values are most likely to be followed by small values and vice versa. α values below 0 are not possible. Since the maximum value for α in DFA m is $m + 1$, higher detrending orders should be used for very non-stationary data with large α . Like in FA and Hurst's analysis, α will decrease or increase by one upon additional differentiation or integration of the data, respectively.

Small deviations from the scaling law (14), i. e. deviations from a straight line in a double logarithmic plot, occur for small scales s , in particular for DFA m with large detrending order m . These deviations are intrinsic to the usual DFA method, since the scaling behaviour is only approached asymptotically. The deviations limit the capability of DFA to determine the correct correlation behaviour in very short records and in the regime of small s . DFA6, e. g., is only defined for $s \geq 8$, and significant deviations from the scaling law $F_2(s) \sim s^\alpha$ occur even up to $s \approx 30$. They will lead to an over-estimation of the fluctuation exponent α , if the regime of small s is used in a fitting procedure. An approach for correction of this systematic artefact in DFA is described in [34].

The number of independent segments of length s is larger in DFA than in WT, and the fluctuations in FA are larger than in DFA. Hence, the analysis has to be based on s values lower than $s_{\max} = N/4$ for DFA compared with $s_{\max} = N/10$ for FA and WT. The accuracy of scaling exponents α determined by DFA was recently studied as a function of the length N of the data [42] (fitting range $s \in [10, N/2]$ was used). The results show that statistical standard errors of α (one standard deviation) are approximately 0.1 for $N = 500$, 0.05 for $N = 3\,000$, and reach 0.03 for $N = 10\,000$. Findings of long-term correlations with $\alpha = 0.6$ in data with only 500 points are thus not significant; and α should be at least 0.55 even for data of 10 000 points.

A generalization of DFA for two-dimensional data (or even higher dimensions d) was recently suggested [33]. The generalization works well when tested with synthetic surfaces including fractional Brownian surfaces and multifractal surfaces. The two-dimensional MF DFA is also adopted to analyse two images from nature and experiment, and nice scaling laws are unravelled. In the 2d procedure, a double cumulative sum (profile) is calculated by summing over both directional indices analogous with Eq. (10), $Y(k, l) = \sum_{i=1}^k \sum_{j=1}^l \tilde{x}_{i,j}$. This surface is partitioned into squares of size $s \times s$ with indices ν and μ , in which polynomials like $y_{\nu,\mu,s}^2(i, j) = ai^2 + bj^2 + cij + di + ej + f$ are fitted. The fluctuation function $F_2(s)$ is again obtained by calculating the variance of the profile from the fits.

5.4 Detection of Trends and Crossovers with DFA

Frequently, the correlations of recorded data do not follow the same scaling law for all time scales s , but one or sometimes even more crossovers between different scaling regimes are observed (see Section 3.3). Time series with a well-defined crossover at s_\times and vanishing correlations above s_\times are most easily generated by Fourier filtering (see Section 8.1). The power spectrum $S(f)$ of an uncorrelated random series is multiplied by $(f/f_\times)^{-\beta}$ with $\beta = 2\alpha - 1$ for frequencies $f > f_\times = 1/s_\times$ only. The series obtained by inverse Fourier transform of this modified power spectrum exhibits power-law correlations on time scales $s < s_\times$ only, while the behaviour becomes uncorrelated on larger time scales $s > s_\times$.

The crossover from $F_2(s) \sim s^\alpha$ to $F_2(s) \sim s^{1/2}$ is clearly visible in double logarithmic plots of the DFA fluctuation function for such short-term correlated data. However, it occurs at times $s_\times^{(m)}$ that are different from the original s_\times used for the generation of the data and that depend on the detrending order m . This systematic deviation is most significant in the DFA m with higher m . Extensive numerical simulations (see Fig. 3 in [34]) show that the ratios of $s_\times^{(m)}/s_\times$ are 1.6, 2.6, 3.6, 4.5, and 5.4 for DFA1, DFA2, ..., DFA5, with an error bar of approximately 0.1. Note, however, that the precise value of this ratio will depend on the method used for fitting the crossover times $s_\times^{(m)}$ (and the method used for generating the data if generated data is analysed). If results for different orders of DFA shall be compared, an observed crossover $s_\times^{(m)}$ can be systematically corrected dividing by the ratio for the corresponding DFA m . If several orders of DFA are used in the procedure, several estimates for the real s_\times will be obtained, which can be checked for consistency or used for an error approximation. A real crossover can thus be well distinguished from the effects of non-stationarities in the data, which

lead to a different dependence of an apparent crossover on m .

The procedure is also required if the characteristic time scale of short-term correlations shall be studied with DFA. If consistent (corrected) s_{\times} values are obtained based on DFA m with different m , the existence of a real characteristic correlation time scale is positively confirmed. Note that lower detrending orders are advantageous in this case, since the observed crossover time scale $s_{\times}^{(m)}$ might become quite large and nearly reach one fourth of the total series length ($N/4$), where the results become statistically inaccurate.

We would like to note that studies showing scaling long-term correlations should not be based on DFA or variants of this method alone in most applications. In particular, if it is not clear whether a given time series is indeed long-term correlated or just short-term correlated with a fairly large crossover time scale, results of DFA should be compared with other methods. For example, one can employ wavelet methods (see, e. g., Section 5.2). Another option is to remove short-term correlations by considering averaged series for comparison. For a time series with daily observations and possible short-term correlations up to two years, for example, one might consider the series of two-year averages and apply DFA together with FA, binned power spectra analysis, and/or wavelet analysis. Only if these methods still indicate long-term correlations, one can be sure that the data are indeed long-term correlated.

As discussed in Section 3.3, records from real measurements are often affected by non-stationarities, and in particular by trends. They have to be well distinguished from the intrinsic fluctuations of the system. To investigate the effect of trends on the DFA m fluctuation functions, one can generate artificial series (\tilde{x}_i) with smooth monotonous trends by adding polynomials of different power p to the original record (x_i),

$$\tilde{x}_i = x_i + Ax^p \quad \text{with } x = i/N. \quad (22)$$

For the DFA m , such trends in the data can lead to an artificial crossover in the scaling behaviour of $F_2(s)$, i. e., the slope α is strongly increased for large time scales s . The position of this artificial crossover depends on the strength A and the power p of the trend. Evidently, no artificial crossover is observed, if the detrending order m is larger than p and p is integer. The order p of the trends in the data can be determined easily by applying the different DFA m . If p is larger than m or p is not an integer, an artificial crossover is observed, the slope α_{trend} in the large s regime strongly depends on m , and the position of the artificial crossover also depends strongly on m . The artificial crossover can thus be clearly distinguished from real crossovers in the correlation behaviour, which result in identical slopes α and rather

similar crossover positions for all detrending orders m . For more extensive studies of trends with non-integer powers we refer to [34, 35]. The effects of periodic trends are also studied in [34].

If the functional form of the trend in given data is not known a priori, the fluctuation function $F_2(s)$ should be calculated for several orders m of the fitting polynomial. If m is too low, $F_2(s)$ will show a pronounced crossover to a regime with larger slope for large scales s [34, 35]. The maximum slope of $\log F_2(s)$ versus $\log s$ is $m + 1$. The crossover will move to larger scales s or disappear when m is increased, unless it is a real crossover not due to trends. Hence, one can find m such that detrending is sufficient. However, m should not be larger than necessary, because shifts of the observed crossover time scales and deviations on short scales s increase with increasing m .

5.5 Sign and Magnitude (Volatility) DFA

To study the origin of long-term fractal correlations in a time series, the series can be split into two parts, which are analysed separately. It is particularly useful to split the series of increments, $\Delta x_i = x_i - x_{i-1}$, $i = 1, \dots, N$, into a series of signs $\tilde{x}_i = s_i = \text{sign} \Delta x_i$ and a series of magnitudes $\tilde{x}_i = m_i = |\Delta x_i|$ [31, 46, 47]. There is an extensive interest in the magnitude time series in economics [48, 49]. These data, usually called volatility, represents the absolute variations in stock (or commodity) prices and are used as a measure quantifying the risk of investments. While the actual prices are only short-term correlated, long-term correlations have been observed in volatility series [48, 49].

Time series having identical distributions and long-range correlation properties can exhibit quite different temporal organizations of the magnitude and sign sub-series. The DFA method can be applied independently to both of these series. Since in particular the signs are often rather strongly anti-correlated and DFA will give incorrect results if α is too close to zero, one often studies integrated sign and magnitude series. As mentioned above, integration $\tilde{x}_i \rightarrow \sum_{j=1}^i \tilde{x}_j$ increases α by one.

Most published results report short-term anti-correlations and no long-term correlations in the sign series, i. e., $\alpha_{\text{sign}} < 1/2$ for the non-integrated signs s_i (or $\alpha_{\text{sign}} < 3/2$ for the integrated signs) on low time scales and $\alpha_{\text{sign}} \rightarrow 1/2$ asymptotically for large s . The magnitude series, on the other hand, are usually either uncorrelated $\alpha_{\text{magn}} = 1/2$ (or $3/2$) or positively long-term correlated $\alpha_{\text{magn}} > 1/2$ (or $3/2$). It has been suggested that findings of $\alpha_{\text{magn}} > 1/2$ are related with nonlinear properties of the data and in particular multifractality [31, 46, 47], if $\alpha < 1.5$ in standard DFA. Specifically, the results suggest that the correlation exponent of the magnitude series

is a monotonically increasing function of the multifractal spectrum (i. e., the singularity spectrum) width of the original series (see Section 6.1). On the other hand, the sign series mainly relates to linear properties of the original series. At small time scales $s < 16$ the standard α is approximately the average of α_{sign} and α_{magn} , if integrated sign and magnitude series are analysed. For $\alpha > 1.5$ in the original series, the integrated magnitude and sign series have approximately the same two-point scaling exponents [46]. An analytical treatment is presented in [47].

5.6 Further Detrending Approaches

A possible drawback of the DFA method is the occurrence of abrupt jumps in the detrended profile $\tilde{Y}_s(j)$ (Eq. (20)) at the boundaries between the segments, since the fitting polynomials in neighbouring segments are not related. A possible way to avoid these jumps would be the calculation of $F_2(s)$ based on polynomial fits in overlapping windows. However, this is rather time consuming due to the polynomial fit in each segment and is consequently not done in most applications. To overcome the problem of jumps several modifications and extensions of the FA and DFA methods have been suggested in the last years. These methods include

- the Detrended Moving Average technique [50, 51, 52], which we denote by Backward Moving Average (BMA) technique (following [53]),
- the Centred Moving Average Average (CMA) method [53], an essentially improved version of BMA,
- the Modified Detrended Fluctuation Analysis (MDFA) [54], which is essentially a mixture of old FA and DFA,
- the continuous DFA (CDFA) technique [55, 56], which is particularly useful for the detection of crossovers,
- the Fourier DFA [57],
- a variant of DFA based on empirical mode decomposition (EMD) [58],
- a variant of DFA based on singular value decomposition (SVD) [59, 60], and
- a variant of DFA based on high-pass filtering [61].

Detrended Moving Average techniques will be thoroughly described and discussed in the next section. A study comparing DFA with CMA and MDFA can be found in [42]. For studies comparing DFA and BMA, see [62, 63]; note that [63] also discusses CMA.

The method we denote as *Modified Detrended Fluctuation Analysis (MDFA)* [54], eliminates trends similar to the DFA method. A polynomial is fitted to the profile function $Y(j)$ in each segment ν and the deviation between the profile function and the polynomial fit is calculated, $\tilde{Y}_s(j) = Y(j) - y_{\nu,s}^p(j)$ (Eq. (20)). To estimate correlations in the data, this method uses a derivative of $\tilde{Y}_s(j)$, obtained for each segment ν , by $\Delta\tilde{Y}_s(j) = \tilde{Y}_s(j+s/2) - \tilde{Y}_s(j)$. Hence, the fluctuation function (compare with Eqs. (13) and (21)) is calculated as follows:

$$F_2(s) = \left[\frac{1}{N} \sum_{j=1}^N \left(\tilde{Y}_s(j+s/2) - \tilde{Y}_s(j) \right)^2 \right]^{1/2}. \quad (23)$$

As in case of DFA, MDFA can easily be generalised to remove higher order trends in the data. Since the fitting polynomials in adjacent segments are not related, $\tilde{Y}_s(j)$ shows abrupt jumps on their boundaries as well. This leads to fluctuations of $F_2(s)$ for large segment sizes s and limits the maximum usable scale to $s < N/4$ as for DFA. The detection of crossovers in the data, however, is more exact with MDFA (compared with DFA), since no correction of the estimated crossover time scales seems to be needed [42].

The *Fourier-detrended fluctuation analysis* [57] aims to eliminate slow oscillatory trends which are found especially in weather and climate series due to seasonal influences. The character of these trends can be rather periodic and regular or irregular, and their influence on the detection of long-range correlations by means of DFA was systematically studied previously [34]. Among other things it has been shown that slowly varying periodic trends disturb the scaling behaviour of the results much stronger than quickly oscillating trends and thus have to be removed prior to the analysis. In case of periodic and regular oscillations, e. g., in temperature fluctuations one simply removes the low frequency seasonal trend by subtracting the daily mean temperatures from the data. Another way, which the Fourier-detrended fluctuation analysis suggests, is to filter out the relevant frequencies in the signals' Fourier spectrum before applying DFA to the filtered signal. Nevertheless, this method faces several difficulties especially its limitation to periodic and regular trends and the need for a priori knowledge of the interfering frequency band.

To study correlations in data with quasi-periodic or irregular oscillating trends, *empirical mode decomposition* (EMD) was suggested [58]. The EMD algorithm breaks down the signal into its intrinsic mode functions (IMFs)

which can be used to distinguish between fluctuations and background. The background, estimated by a quasi-periodic fit containing the dominating frequencies of a sufficiently large number of IMFs, is subtracted from the data, yielding a slightly better scaling behaviour in the DFA curves. However, we believe that the method might be too complicated for wide-spread applications.

Another method which was shown to minimise the effect of periodic and quasi-periodic trends is based on *singular value decomposition* (SVD) [59, 60]. In this approach, one first embeds the original signal in a matrix whose dimension has to be much larger than the number of frequency components of the periodic or quasi-periodic trends obtained in the power spectrum. Applying SVD yields a diagonal matrix which can be manipulated by setting the dominant eigen-values (associated with the trends) to zero. The filtered matrix finally leads to the filtered data, and it has been shown that subsequent application of DFA determines the expected scaling behaviour if the embedding dimension is sufficiently large. None the less, the performance of this rather complex method seems to decrease for larger values of the scaling exponent. Furthermore SVD-DFA assumes that trends are deterministic and narrow banded.

The detrending procedure in DFA (Eq. (20)) can be regarded as a scale-dependent high-pass filter since (low-frequency) fluctuations exceeding a specific scale s are eliminated. Therefore, it has been suggested to obtain the detrended profile $\tilde{Y}_s(j)$ for each scale s directly by applying digital high-pass filters [61]. In particular, Butterworth, Chebyshev-I, Chebyshev-II, and an elliptical filter were suggested. While the elliptical filter showed the best performance in detecting long-range correlations in artificial data, the Chebyshev-II filter was found to be problematic. Additionally, in order to avoid a time shift between filtered and original profile, the average of the directly filtered signal and the time reversed filtered signal is considered. The effects of these complicated filters on the scaling behaviour are, however, not fully understood.

Finally, a continuous DFA method has been suggested in the context of studying heartbeat data during sleep [55, 56]. The method compares unnormalised fluctuation functions $F_2(s)$ for increasing length of the data. I. e., one starts with a very short recording and subsequently adds more points of data. The method is particularly suitable for the detection of change points in the data, e. g., physiological transitions between different activity or sleep stages. Since the main objective of the method is not the study of scaling behaviour, we do not discuss it in detail here.

5.7 Centered Moving Average (CMA) Analysis

Particular attractive modifications of DFA are the *Detrended Moving Average* (DMA) methods, where running averages replace the polynomial fits. The first suggested version, the *Backward Moving Average* (BMA) method [50, 51, 52], however, suffers from severe problems, because an artificial time shift of s between the original signal and the moving average is introduced. This time shift leads to an additional contribution to the detrended profile $\tilde{Y}_s(j)$, which causes a larger fluctuation function $F_2(s)$ in particular for small scales in the case of long-term correlated data. Hence, the scaling exponent α is systematically underestimated [62]. In addition, the BMA method performs even worse for data with trends [63], and its slope is limited by $\alpha < 1$ just as for the non-detrending method FA.

It was soon recognised that the intrinsic error of BMA can be overcome by eliminating the artificial time shift. This leads to the *Centred Moving Average* (CMA) method [53], where $\tilde{Y}_s(j)$ is calculated as

$$\tilde{Y}_s(j) = Y(j) - \frac{1}{s} \sum_{i=-(s-1)/2}^{(s-1)/2} Y(j+i), \quad (24)$$

replacing Eq. (20) while Eq. (21) and the rest of the DFA procedure described in Section 5.3 stay the same. Unlike DFA, the CMA method cannot easily be generalised to remove linear and higher order trends in the data.

It was recently proposed [42] that the scaling behaviour of the CMA method is more stable than for DFA1 and MDFA1, suggesting that CMA could be used for reliable computation of α even for scales $s < 10$ (without correction of any systematic deviations needed in DFA for this regime) and up to $s_{\max} = N/2$. The standard errors in determining the scaling exponent α by fitting straight lines to the double logarithmic plots of $F_2(s)$ have been studied in [42]; they are comparable with DFA1 (see end of Section 5.3).

Regarding the determination of crossovers, CMA is comparable to DFA1. Ultimately, the CMA seems to be a good alternative to DFA1 when analysing the scaling properties in short data sets without trends. Nevertheless for data with possible unknown trends we recommend the application of standard DFA with several different detrending polynomial orders in order to distinguish real crossovers from artificial crossovers due to trends. In addition, an independent approach (e. g., wavelet analysis) should be used to confirm findings of long-term correlations (see also Section 5.4).

6 Methods for Multifractal Time Series Analysis

This chapter describes the multifractal characterisation of time series, for an introduction, see Section 3.4. The simplest type of multifractal analysis is based upon the standard partition function multifractal formalism, which has been developed for the multifractal characterisation of normalised, stationary measures [6, 12, 64, 65]. Unfortunately, this standard formalism does not give correct results for non-stationary time series that are affected by trends or that cannot be normalised. Thus, in the early 1990s an improved multifractal formalism has been developed, the wavelet transform modulus maxima (WTMM) method [66, 67, 68, 69, 70], which is based on wavelet analysis and involves tracing the maxima lines in the continuous wavelet transform over all scales. An important alternative is the multifractal DFA (MF-DFA) algorithm [32], which does not require the modulus maxima procedure, and hence involves little more effort in programming than the conventional DFA. For studies comparing methods for detrending multifractal analysis (multifractal DFA (MF-DFA) and wavelet transform modulus maxima (WTMM) method), see [32, 71, 72].

6.1 The Structure Function Approach and Singularity Spectra

In the general multifractal formalism, one considers a normalised measure $\mu(t)$, $t \in [0, 1]$, and defines the box probabilities $\tilde{\mu}_s(t) = \int_{t-s/2}^{t+s/2} \mu(t') dt'$ in neighbourhoods of (scale) length $s \ll 1$ around t . The multifractal approach is then introduced by the partition function

$$Z_q(s) = \sum_{\nu=0}^{1/s-1} \tilde{\mu}_s^q[(\nu + 1/2)s] \sim s^{\tau(q)} \quad \text{for } s \ll 1, \quad (25)$$

where $\tau(q)$ is the Renyi scaling exponent and q is a real parameter that can take positive as well as negative moments. Note that $\tau(q)$ is sometimes defined with opposite sign (see, e. g., [6]). A record is called monofractal (or self-affine), when the Renyi scaling exponent $\tau(q)$ depends linearly on q ; otherwise it is called multifractal. The generalised multifractal dimensions $D(q)$ (see also Section 3.4) are related to $\tau(q)$ by $D(q) = \tau(q)/q - 1$, such that the fractal dimension of the support is $D(0) = -\tau(0)$ and the correlation dimension is $D(2) = \tau(2)$.

In time series, a discrete version has to be used, and the considered data (x_i) , $i = 1, \dots, N$ may usually include negative values. Hence, setting $N_s =$

$\text{int}(N/s)$ and $X(\nu, s) = \sum_{i=1}^s x_{\nu s+i}$ for $\nu = 0, \dots, N_s - 1$ we can define [6, 12],

$$Z_q(s) = \sum_{\nu=0}^{N_s-1} |X(\nu, s)|^q \sim s^{\tau(q)} \quad \text{for } s > 1. \quad (26)$$

Inserting the profile $Y(j)$ and $F_{\text{FA}}(\nu, s)$ from Eqs. (10) and (11), respectively, we obtain

$$Z_q(s) = \sum_{\nu=0}^{N_s-1} \left\{ [Y((\nu+1)s) - Y(\nu s)]^2 \right\}^{q/2} = \sum_{\nu=0}^{N_s-1} F_{\text{FA}}^{q/2}(\nu, s). \quad (27)$$

Comparing Eqs. (27) with (13), we see that this multifractal approach can be considered as a generalised version of the Fluctuation Analysis (FA) method, where the exponent 2 is replaced by q . In particular we find (disregarding the summation over the second partition of the time series)

$$F_2(s) \sim \left[\frac{1}{N_s} Z_2(s) \right]^{1/2} \sim s^{[1+\tau(2)]/2} \Rightarrow 2\alpha = 1 + \tau(2) = 1 + D(2). \quad (28)$$

We thus see that all methods for (mono-)fractal time analysis (discussed in Chapters 4 and 5) in fact study the correlation dimension $D(2) = 2\alpha - 1 = \beta = 1 - \gamma$ (see Eq. (15)).

It is straightforward to define a generalised (multifractal) Hurst exponent $h(q)$ for the scaling behaviour of the q th moments of the fluctuations [64, 65],

$$F_q(s) = \left[\frac{1}{N_s} Z_2(s) \right]^{1/q} \sim s^{[1+\tau(q)]/q} = s^{h(q)} \Rightarrow h(q) = \frac{1 + \tau(q)}{q}. \quad (29)$$

with $h(2) = \alpha \approx H$. In the following, we will use only $h(2)$ for the standard fluctuation exponent (denoted by α in the previous chapters), and reserve the letter α for the Hölder exponent.

Another way to characterise a multifractal series is the singularity spectrum $f(\alpha)$, that is related to $\tau(q)$ via a Legendre transform [6, 12],

$$\alpha = \frac{d}{dq} \tau(q) \quad \text{and} \quad f(\alpha) = q\alpha - \tau(q). \quad (30)$$

Here, α is the singularity strength or Hölder exponent (see also articles ... in the encyclopedia), while $f(\alpha)$ denotes the dimension of the subset of the series that is characterised by α . Note that α is *not* the fluctuation scaling exponent in this section, although the same letter is traditionally used for both. Using Eq. (29), we can directly relate α and $f(\alpha)$ to $h(q)$,

$$\alpha = h(q) + qh'(q) \quad \text{and} \quad f(\alpha) = q[\alpha - h(q)] + 1. \quad (31)$$

6.2 Wavelet Transform Modulus Maxima (WTMM) Method

The wavelet transform modulus maxima (WTMM) method [66, 67, 68, 69, 70] is a well-known method to investigate the multifractal scaling properties of fractal and self-affine objects in the presence of non-stationarities. For applications, see e. g. [73, 74]. It is based upon the wavelet transform with continuous basis functions as defined in Section 5.1, Eq. (16). Note that in this case the series \tilde{x}_i are analysed directly instead of the profile $Y(j)$ defined in Eq. (10). Using wavelets orthogonal to m th order polynomials, the corresponding trends are eliminated.

Instead of averaging over all wavelet coefficients $L_\psi(\tau, s)$, one averages, within the modulo-maxima method, only the local maxima of $|L_\psi(\tau, s)|$. First, one determines for a given scale s , the positions τ_j of the local maxima of $|W(\tau, s)|$ as function of τ , so that $|L_\psi(\tau_j - 1, s)| < |L_\psi(\tau_j, s)| \geq |L_\psi(\tau_j + 1, s)|$ for $j = 1, \dots, j_{\max}$. This maxima procedure is demonstrated in Fig. 7. Then one sums up the q th power of the maxima,

$$Z(q, s) = \sum_{j=1}^{j_{\max}} |L_\psi(\tau_j, s)|^q. \quad (32)$$

The reason for the maxima procedure is that the absolute wavelet coefficients $|L_\psi(\tau, s)|$ can become arbitrarily small. The analysing wavelet $\psi(x)$ must always have positive values for some x and negative values for other x , since it has to be orthogonal to possible constant trends. Hence there are always positive and negative terms in the sum (16), and these terms might cancel. If that happens, $|L_\psi(\tau, s)|$ can become close to zero. Since such small terms would spoil the calculation of negative moments in Eq. (32), they have to be eliminated by the maxima procedure.

In fluctuation analysis, on the other hand, the calculation of the variances $F^2(\nu, s)$, e. g. in Eq. (11), involves only positive terms under the summation. The variances cannot become arbitrarily small, and hence no maximum procedure is required for series with compact support. In addition, the variances will always increase if the segment length s is increased, because the fit will always be worse for a longer segment. In the WTMM method, in contrast, the absolute wavelet coefficients $|L_\psi(\tau, s)|$ need not increase with increasing scale s , even if only the local maxima are considered. The values $|L_\psi(\tau, s)|$ might become smaller for increasing s since just more (positive and negative) terms are included in the summation (16), and these might cancel even better. Thus, an additional supremum procedure has been introduced in the WTMM method in order to keep the dependence of $Z(q, s)$

on s monotonous. If, for a given scale s , a maximum at a certain position τ_j happens to be smaller than a maximum at $\tau'_j \approx \tau_j$ for a lower scale $s' < s$, then $L_\psi(\tau_j, s)$ is replaced by $L_\psi(\tau'_j, s')$ in Eq. (32).

Often, scaling behaviour is observed for $Z(q, s)$, and scaling exponents $\hat{\tau}(q)$ can be defined that describe how $Z(q, s)$ scales with s ,

$$Z(q, s) \sim s^{\hat{\tau}(q)}. \quad (33)$$

The exponents $\hat{\tau}(q)$ characterise the multifractal properties of the series under investigation, and theoretically they are identical with the $\tau(q)$ defined in Eq. (26) [66, 67, 68, 70] and related to $h(q)$ by Eq. (29).

6.3 Multifractal Detrended Fluctuation Analysis (MF-DFA)

The multifractal DFA (MF-DFA) procedure consists of five steps [32]. The first three steps are essentially identical to the conventional DFA procedure (see Section 5.3 and Fig. 4). Let us assume that (\tilde{x}_i) is a series of length N , and that this series is of compact support. The support can be defined as the set of the indices j with nonzero values \tilde{x}_j , and it is compact if $\tilde{x}_j = 0$ for an insignificant fraction of the series only. The value of $\tilde{x}_j = 0$ is interpreted as having no value at this j . Note that we are *not* discussing the fractal or multifractal features of the plot of the time series in a two-dimensional graph (see also the discussion in Section 3.1), but analysing time series as one-dimensional structures with values assigned to each point. Since real time series always have finite length N , we explicitly want to determine the multifractality of finite series, and we are not discussing the limit for $N \rightarrow \infty$ here (see also Section 6.1).

- *Step 1:* Calculate the profile $Y(j)$, Eq. (10), by integrating the time series.
- *Step 2:* Divide the profile $Y(j)$ into $N_s = \text{int}(N/s)$ non-overlapping segments of equal length s . Since the length N of the series is often not a multiple of the considered time scale s , the same procedure can be repeated starting from the opposite end. Thereby, $2N_s$ segments are obtained altogether.
- *Step 3:* Calculate the local trend for each of the $2N_s$ segments by a least-square fit of the profile. Then determine the variance by Eqs. (20)

and (21) for each segment $\nu = 0, \dots, 2N_s - 1$. Again, linear, quadratic, cubic, or higher order polynomials can be used in the fitting procedure, and the corresponding methods are thus called MF-DFA1, MF-DFA2, MF-DFA3, ... [32]. In (MF-)DFA m [m th order (MF-)DFA] trends of order mp in the profile (or, equivalently, of order $m - 1$ in the original series) are eliminated. Thus a comparison of the results for different orders of DFA allows one to estimate the type of the polynomial trend in the time series [34, 35].

- *Step 4:* Average over all segments to obtain the q th order fluctuation function

$$F_q(s) = \left\{ \frac{1}{2N_s} \sum_{\nu=1}^{2N_s} [F_{\text{DFA}m}^2(\nu, s)]^{q/2} \right\}^{1/q}, \quad (34)$$

This is the generalization of Eq. (13) suggested by the relations derived in Section 6.1. For $q = 2$, the standard DFA procedure is retrieved. One is interested in how the generalised q dependent fluctuation functions $F_q(s)$ depend on the time scale s for different values of q . Hence, we must repeat steps 2 to 4 for several time scales s . It is apparent that $F_q(s)$ will increase with increasing s . Of course, $F_q(s)$ depends on the order m . By construction, $F_q(s)$ is only defined for $s \geq m + 2$.

- *Step 5:* Determine the scaling behaviour of the fluctuation functions by analysing log-log plots $F_q(s)$ versus s for each value of q . If the series \tilde{x}_i are long-range power-law correlated, $F_q(s)$ increases, for large values of s , as a power-law,

$$F_q(s) \sim s^{h(q)} \quad \text{with} \quad h(q) = \frac{1 + \tau(q)}{q}. \quad (35)$$

For very large scales, $s > N/4$, $F_q(s)$ becomes statistically unreliable because the number of segments N_s for the averaging procedure in step 4 becomes very small. Thus, scales $s > N/4$ should be excluded from the fitting procedure determining $h(q)$. Besides that, systematic deviations from the scaling behaviour in Eq. (35), which can be corrected, occur for small scales $s \approx 10$.

The value of $h(0)$, which corresponds to the limit $h(q)$ for $q \rightarrow 0$, cannot be determined directly using the averaging procedure in Eq. (34) because of the diverging exponent. Instead, a logarithmic averaging procedure has to

be employed,

$$F_0(s) = \exp \left\{ \frac{1}{4N_s} \sum_{\nu=1}^{2N_s} \ln [F^2(\nu, s)] \right\} \sim s^{h(0)}. \quad (36)$$

Note that $h(0)$ cannot be defined for time series with fractal support, where $h(q)$ diverges for $q \rightarrow 0$.

For monofractal time series with compact support, $h(q)$ is independent of q , since the scaling behaviour of the variances $F_{\text{DFAm}}^2(\nu, s)$ is identical for all segments ν , and the averaging procedure in Eq. (34) will give just this identical scaling behaviour for all values of q . Only if small and large fluctuations scale differently, there will be a significant dependence of $h(q)$ on q : If we consider positive values of q , the segments ν with large variance $F^2(\nu, s)$ (i. e. large deviations from the corresponding fit) will dominate the average $F_q(s)$. Thus, for positive values of q , $h(q)$ describes the scaling behaviour of the segments with large fluctuations. On the contrary, for negative values of q , the segments ν with small variance $F_{\text{DFAm}}^2(\nu, s)$ will dominate the average $F_q(s)$. Hence, for negative values of q , $h(q)$ describes the scaling behaviour of the segments with small fluctuations. Figure 8 shows typical results obtained for $F_q(s)$ in the MF-DFA procedure.

Usually the large fluctuations are characterised by a smaller scaling exponent $h(q)$ for multifractal series than the small fluctuations. This can be understood from the following arguments: For the maximum scale $s = N$ the fluctuation function $F_q(s)$ is independent of q , since the sum in Eq. (34) runs over only two identical segments. For smaller scales $s \ll N$ the averaging procedure runs over several segments, and the average value $F_q(s)$ will be dominated by the $F^2(\nu, s)$ from the segments with small (large) fluctuations if $q < 0$ ($q > 0$). Thus, for $s \ll N$, $F_q(s)$ with $q < 0$ will be smaller than $F_q(s)$ with $q > 0$, while both become equal for $s = N$. Hence, if we assume an homogeneous scaling behaviour of $F_q(s)$ following Eq. (35), the slope $h(q)$ in a log-log plot of $F_q(s)$ with $q < 0$ versus s must be larger than the corresponding slope for $F_q(s)$ with $q > 0$. Thus, $h(q)$ for $q < 0$ will usually be larger than $h(q)$ for $q > 0$.

However, the MF-DFA method can only determine *positive* generalised Hurst exponents $h(q)$, and it already becomes inaccurate for strongly anti-correlated signals when $h(q)$ is close to zero. In such cases, a modified (MF-)DFA technique has to be used. The most simple way to analyse such data is to integrate the time series before the MF-DFA procedure. Following the MF-DFA procedure as described above, we obtain a generalised fluctuation functions described by a scaling law with $\tilde{h}(q) = h(q) + 1$. The scaling behaviour can thus be accurately determined even for $h(q)$ which are smaller than zero for some values of q .

The accuracy of $h(q)$ determined by MF-DFA certainly depends on the length N of the data. For $q = \pm 10$ and data with $N = 10\,000$ and $100\,000$, systematic and statistical error bars (standard deviations) up to $\Delta h(q) \approx \pm 0.1$ and $\approx \pm 0.05$ should be expected, respectively [32]. A difference of $h(-10) - h(+10) = 0.2$, corresponding to an even larger width $\Delta\alpha$ of the singularity spectrum $f(\alpha)$ defined in Eq. (30) is thus not significant unless the data was longer than $N = 10\,000$ points. Hence, one has to be very careful when concluding multifractal properties from differences in $h(q)$.

As already mentioned in the introduction, two types of multifractality in time series can be distinguished. Both of them require a multitude of scaling exponents for small and large fluctuations: (i) Multifractality of a time series can be due to a broad probability density function for the values of the time series, and (ii) multifractality can also be due to different long-range correlations for small and large fluctuations. The most easy way to distinguish between these two types is by analysing also the corresponding randomly shuffled series [32]. In the shuffling procedure the values are put into random order, and thus all correlations are destroyed. Hence the shuffled series from multifractals of type (ii) will exhibit simple random behaviour, $h_{\text{shuf}}(q) = 0.5$, i. e. non-multifractal scaling. For multifractals of type (i), on the contrary, the original $h(q)$ dependence is not changed, $h(q) = h_{\text{shuf}}(q)$, since the multifractality is due to the probability density, which is not affected by the shuffling procedure. If both kinds of multifractality are present in a given series, the shuffled series will show weaker multifractality than the original one.

6.4 Comparison of WTMM and MF-DFA

The MF-DFA results turn out to be slightly more reliable than the WTMM results [32, 71, 72]. In particular, the MF-DFA has slight advantages for negative q values and short series. In the other cases the results of the two methods are rather equivalent. Besides that, the main advantage of the MF-DFA method compared with the WTMM method lies in the simplicity of the MF-DFA method. However, contrary to WTMM, MF-DFA is restricted to studies of data with full one-dimensional support, while WTMM is not. Both, WTMM and MF-DFA have been generalised for higher dimensional data, see [33] for higher dimensional MF-DFA and, e. g., [70] for higher dimensional WTMM. Studies of other generalisations of detrending methods like the discrete WT approach (see Section 5.2) and the CMA method (see Section 5.7) are currently under investigation [75].

7 Statistics of Extreme Events in Fractal Time Series

The statistics of return intervals between well defined extremal events is a powerful tool to characterise the temporal scaling properties of observed time series and to derive quantities for the estimation of the risk for hazardous events like floods, very high temperatures, or earthquakes. It was shown recently that long-term correlations represent a natural mechanism for the clustering of the hazardous events [76]. In this chapter we will discuss the most important consequences of long-term correlations and fractal scaling of time series upon the statistics of extreme events [76, 77, 78, 79, 80]. Corresponding work regarding multifractal data [81] is not discussed here.

7.1 Return Intervals Between Extreme Events

To study the statistics of return intervals we consider again a time series (x_i) , $i = 1, \dots, N$ with fractal scaling behaviour, sampled homogeneously and normalised to zero mean and unit variance. For describing the reoccurrence of rare events exceeding a certain threshold q , we investigate the return intervals r_q between these events, see Fig. 9. The average return interval $R_q = \langle r_q \rangle$ increases as a function of the threshold q (see, e. g. [82]). It is known that for uncorrelated records ('white noise'), the return intervals are also uncorrelated and distributed according to the Poisson distribution, $P_q(r) = \frac{1}{R_q} \exp(-r/R_q)$. For fractal (long-term correlated) data with auto-correlations following Eq. (5), we obtain a *stretched* exponential [76, 77, 78, 79, 83],

$$P_q(r) = \frac{a_\gamma}{R_q} \exp[-b_\gamma(r/R_q)^\gamma], \quad (37)$$

This behaviour is shown in Fig. 10. The exponent γ is the correlation exponent from $C(s)$, and the parameters a_γ and b_γ are independent of q . They can be determined from the normalization conditions for $P_q(r)$, i. e., $\int P_q(r) dr = 1$ and $\int r P_q(r) dr = R_q$. The form of the distribution (37) indicates that return intervals both well below and well above their average value R_q (which is independent of γ) are considerably more frequent for long-term correlated than for uncorrelated data. It has to be noted that there are deviations from the stretched exponential law (37) for very small r (discretization effects and an additional power-law regime) and for very large r (finite size effects), see Fig. 10. The extent of the deviations from Eq. (37) depends on the distribution of the values x_i of the time series. For a discussion of these effects, see [79].

Equation (37) does not quantify, however, if the return intervals themselves are arranged in a correlated or in an uncorrelated fashion, and if clustering of rare events may be induced by long-term correlations. To study this question, one has to evaluate the auto-correlation function $C_r(s) = \langle r_q(l)r_q(l+s) \rangle - R_q^2$ of the return intervals. The results for model data suggests that also the return intervals are long-term power-law correlated, with the same exponent γ as the original record. Accordingly, large and small return intervals are not arranged in a random fashion but are expected to form clusters. As a consequence, the probability of finding a certain return interval r depends on the value of the preceding interval r_0 , and this effect has to be taken into account in predictions and risk estimations [76, 79].

The conditional distribution function $P_q(r|r_0)$ is a basic quantity, from which the relevant quantities in risk estimations can be derived [82]. For example, the first moment of $P_q(r|r_0)$ is the average value $R_q(r_0)$ of those return intervals that directly follow r_0 . By definition, $R_q(r_0)$ is the expected waiting time to the next event, when the two events before were separated by r_0 . The more general quantity is the expected waiting time $\tau_q(x|r_0)$ to the next event, when the time x has been elapsed. For $x = 0$, $\tau_q(0|r_0)$ is identical to $R_q(r_0)$. In general, $\tau_q(x|r_0)$ is related to $P_q(r|r_0)$ by

$$\tau_q(x|r_0) = \int_x^\infty (r-x)P_q(r|r_0)dr / \int_x^\infty P_q(r|r_0)dr \quad (38)$$

For uncorrelated records, $\tau_q(x|r_0)/R_q = 1$ (except for discreteness effects that lead to $\tau_q(x|r_0)/R_q > 1$ for $x > 0$, see [84]). Due to the scaling of $P_q(r|r_0)$, also $\tau_q(x|r_0)/R_q$ scales with r_0/R_q and x/R_q . Small and large return intervals are more likely to be followed by small and large ones, respectively, and hence $\tau_q(0|r_0)/R_q = R_q(r_0)/R_q$ is well below (above) one for r_0/R_q well below (above) one. With increasing x , the expected residual time to the next event increases. Note that only for an infinite long-term correlated record, the value of $\tau_q(x|r_0)$ will increase indefinitely with x and r_0 . For real (finite) records, there exists a maximum return interval which limits the values of x , r_0 and $\tau_q(x|r_0)$.

7.2 Distribution of Extreme Events

In this section we describe how the presence of fractal long-term correlations affects the statistics of the extreme events, i. e., maxima within time segments of fixed duration R , see Fig. 11 for illustration. By definition, extreme events are rare occurrences of extraordinary nature, such as, e. g. floods, very high temperatures, or earthquakes. In hydrological engineering such conventional extreme value statistics are commonly applied to decide what

building projects are required to protect riverside areas against typical floods that occur for example once in 100 years. Most of these results are based on statistically independent values x_i and hold only in the limit $R \rightarrow \infty$. However, both of these assumptions are not strictly fulfilled for correlated fractal scaling data.

In classical extreme value statistics one assumes that records (x_i) consist of i.i.d. data, described by density distributions $P(x)$, which can be, e. g., a Gaussian or an exponential distribution. One is interested in the distribution density function $P_R(m)$ of the maxima (m_j) determined in segments of length R in the original series (x_i) , see Fig. 11. Note that all maxima are also elements of the original data. The corresponding integrated maxima distribution $G_R(m)$ is defined as

$$G_R(m) = 1 - E_R(m) = \int_{-\infty}^m P_R(m') dm'. \quad (39)$$

Since $G_R(m)$ is the probability of finding a maximum smaller than m , $E_R(m)$ denotes the probability of finding a maximum that exceeds m . One of the main results of traditional extreme value statistics states that for independently and identically distributed (i.i.d.) data (x_i) with Gaussian or exponential distribution density function $P(x)$ the integrated distribution $G_R(m)$ converges to a double exponential (Fisher-Tippet-Gumbel) distribution (often labelled as Type I) [85, 86, 87, 88, 89], i. e.,

$$G_R(m) \rightarrow G\left(\frac{m-u}{\alpha}\right) = \exp\left[-\exp\left(-\frac{m-u}{\alpha}\right)\right] \quad (40)$$

for $R \rightarrow \infty$, where α is the scale parameter and u the location parameter. By the method of moments those parameters are given by $\alpha = \frac{\sqrt{6}}{\pi}\sigma_R$ and $u = m_R - n_e\alpha$ with the Euler constant $n_e = 0.577216$ [88, 90, 91, 92]. Here m_R and σ_R denote the (R -dependent) mean maximum and the standard deviation, respectively. Note that different asymptotics will be reached for broader distributions of data (x_i) that belong to other domains of attraction [88]. For example, for data following a power-law distribution (or Pareto distribution), $P(x) = (x/x_0)^{-k}$, $G_R(m)$ converges to a Fréchet distribution, often labelled as Type II. For data following a distribution with finite upper endpoint, for example the uniform distribution $P(x) = 1$ for $0 \leq x \leq 1$, $G_R(m)$ converges to a Weibull distribution, often labelled as Type III. We do not consider the latter two types of asymptotics here.

Numerical studies of fractal model data have recently shown that the distribution $P(x)$ of the original data has a much stronger effect upon the convergence towards the Gumbel distribution than the long-term correlations in the data. Long-term correlations just slightly delay the convergence

of $G_R(m)$ towards the Gumbel distribution (40). This can be observed very clearly in a plot of the integrated and scaled distribution $G_R(m)$ on logarithmic scale [80].

Furthermore, it was found numerically that (i) the maxima series (m_j) exhibit long-term correlations similar to those of the original data (x_i), and most notably (ii) the maxima distribution as well as the mean maxima significantly depend on the history, in particular on the previous maximum [80]. The last item implies that conditional mean maxima and conditional maxima distributions should be considered for improved extreme event predictions.

8 Simple Models for Fractal and Multifractal Time Series

8.1 Fourier Filtering

Fractal scaling with long-term correlations can be introduced most easily into time series by the Fourier-filtering technique, see, e. g., [93, 94, 95]. The Fourier filtering technique is not limited to the generation of long-term correlated data characterised by a power-law auto-correlation function $C(s) \sim s^{-\gamma}$ with $0 < \gamma < 1$. All values of the scaling exponents $\alpha = h(2) \approx H$ or $\beta = 2\alpha - 1$ can be obtained, even those that cannot be found directly by the fractal analysis techniques described in Chapters 4 and 5 (e. g. $\alpha < 1$). Note, however, that Fourier filtering will always yield Gaussian distributed data values and that no nonlinear or multifractal properties can be achieved (see also Sections 3.4, 5.5, and Chapter 6). In Section 5.4, we have briefly described a modification of Fourier filtering for obtaining reliable short-term correlated data.

For the generation of data characterised by fractal scaling with $\beta = 2\alpha - 1$ [93, 94] we start with uncorrelated Gaussian distributed random numbers x_i from an i.i.d. generator. Transforming a series of such numbers into frequency space with discrete Fourier transform or FFT (for suitable series lengths N) yields a flat power spectrum, since random numbers correspond to white noise. Multiplying the (complex) Fourier coefficients by $f^{-\beta/2}$, where $f \propto 1/s$ is the frequency, will rescale the power spectrum $S(f)$ to follow Eq. (6), as expected for time series with fractal scaling. After transforming back to the time domain (using inverse Fourier transform or inverse FFT) we will thus obtain the desired long-term correlated data \tilde{x}_i . The final step is the normalization of this data.

The Fourier filtering method can be improved using modified Bessel functions instead of the simple factors $f^{-\beta/2}$ in modifying the Fourier coefficients

[95]. This way problems with the divergence of the autocorrelation function $C(s)$ at $s = 0$ can be avoided.

An alternative method to the Fourier filtering technique, the random midpoint displacement method, is based on the construction of self-affine surfaces by an iterative procedure, see, e. g. [6]. Starting with one interval with constant values, the intervals are iterative split in the middle and the midpoint is displaced by a random offset. The amplitude of this offset is scaled according to the length of the interval. Since the method generates a self-affine surface x_i characterised by a Hurst exponent H , the differentiated series Δx_i can be used as long-term correlated or anti-correlated random numbers. Note, however, that the correlations do not persist for the whole length of the data generated this way. Another option is the use of wavelet synthesis, the reverse of wavelet analysis described in Section 5.1. In that method, the scaling law is introduced by setting the magnitudes of the wavelet coefficients according to the corresponding time scale s .

8.2 The Schmitz-Schreiber Method

When long-term correlations in random numbers are introduced by the Fourier-filtering technique (see previous section), the original distribution $P(x)$ of the time series values x_i is always modified such that it becomes closer to a Gaussian. Hence, no series (x_i) with broad distributions of the values *and* fractal scaling can be generated. In these cases an iterative algorithm introduced by Schreiber and Schmitz [97, 98] must be applied.

The algorithm consists of the following steps: First one creates a Gaussian distributed long-term correlated data set with the desired correlation exponent γ by standard Fourier-filtering [95]. The power spectrum $S_G(f) = F_G(f)F_G^*(f)$ of this data set is considered as reference spectrum (where f denotes the frequency in Fourier space and the $F_G(f)$ are the complex Fourier coefficients). Next one creates an uncorrelated sequence of random numbers (x_i^{ref}) , following a desired distribution $P(x)$. The (complex) Fourier transform $F(f)$ of the (x_i^{ref}) is now divided by its absolute value and multiplied by the square root of the reference spectrum,

$$F_{\text{new}}(f) = \frac{F(f)\sqrt{S_G(f)}}{|F(f)|}. \quad (41)$$

After the Fourier back-transformation of $F_{\text{new}}(f)$, the new sequence (x_i^{new}) has the desired correlations (i. e. the desired γ), but the shape of the distribution has changed towards a (more or less) Gaussian distribution. In order to enforce the desired distribution, we exchange the (x_i^{new}) by the (x_i^{ref}) , such

that the largest value of the new set is replaced by the largest value of the reference set, the second largest of the new set by the second largest of the reference set and so on. After this the new sequence has the desired distribution and is clearly correlated. However, due to the exchange algorithm the perfect long-term correlations of the new data sequence were slightly altered again. So the procedure is repeated: the new sequence is Fourier transformed followed by spectrum adjustment, and the exchange algorithm is applied to the Fourier back-transformed data set. These steps are repeated several times, until the desired quality (or the best possible quality) of the spectrum of the new data series is achieved.

8.3 The Extended Binomial Multifractal Model

The multifractal cascade model [6, 64, 32] is a standard model for multifractal data, which is often applied, e. g., in hydrology [96]. In the model, a record x_i of length $N = 2^{n_{\max}}$ is constructed recursively as follows. In generation $n = 0$, the record elements are constant, i. e. $x_i = 1$ for all $i = 1, \dots, N$. In the first step of the cascade (generation $n = 1$), the first half of the series is multiplied by a factor a and the second half of the series is multiplied by a factor b . This yields $x_i = a$ for $i = 1, \dots, N/2$ and $x_i = b$ for $i = N/2 + 1, \dots, N$. The parameters a and b are between zero and one, $0 < a < b < 1$. One need not restrict the model to $b = 1 - a$ as is often done in the literature [6]. In the second step (generation $n = 2$), we apply the process of step 1 to the two subseries, yielding $x_i = a^2$ for $i = 1, \dots, N/4$, $x_i = ab$ for $i = N/4 + 1, \dots, N/2$, $x_i = ba = ab$ for $i = N/2 + 1, \dots, 3N/4$, and $x_i = b^2$ for $i = 3N/4 + 1, \dots, N$. In general, in step $n + 1$, each subseries of step n is divided into two subseries of equal length, and the first half of the x_i is multiplied by a while the second half is multiplied by b . For example, in generation $n = 3$ the values in the eight subseries are a^3 , a^2b , a^2b , ab^2 , a^2b , ab^2 , ab^2 , b^3 . After n_{\max} steps, the final generation has been reached, where all subseries have length 1 and no more splitting is possible. We note that the final record can be written as $x_i = a^{n_{\max} - n(i-1)} b^{n(i-1)}$, where $n(i)$ is the number of digits 1 in the binary representation of the index i , e. g. $n(13) = 3$, since 13 corresponds to binary 1101.

For this multiplicative cascade model, the formula for $\tau(q)$ has been derived earlier [6, 64, 32]. The result is $\tau(q) = [-\ln(a^q + b^q) + q \ln(a + b)] / \ln 2$ or

$$h(q) = \frac{1}{q} - \frac{\ln(a^q + b^q)}{q \ln 2} + \frac{\ln(a + b)}{\ln 2}. \quad (42)$$

It is easy to see that $h(1) = 1$ for all values of a and b . Thus, in this form the model is limited to cases where $h(1)$, which is the exponent Hurst defined

originally in the R/S method, is equal to one.

In order to generalise this multifractal cascade process such that any value of $h(1)$ is possible, one can subtract the offset $\Delta h = \ln(a+b)/\ln(2)$ from $h(q)$ [99]. The constant offset Δh corresponds to additional long-term correlations incorporated in the multiplicative cascade model. For generating records without this offset, we rescale the power spectrum. First, we fast-Fourier transform (FFT) the simple multiplicative cascade data into the frequency domain. Then, we multiply all Fourier coefficients by $f^{-\Delta h}$, where f is the frequency. This way, the slope β of the power spectra $S(f) \sim f^{-\beta}$ is decreased from $\beta = 2h(2) - 1 = [2\ln(a+b) - \ln(a^2+b^2)]/\ln 2$ into $\beta' = 2[h(2) - \Delta h] - 1 = -\ln(a^2+b^2)/\ln 2$. Finally, backward FFT is employed to transform the signal back into the time domain.

8.4 The Bi-fractal Model

In some cases a simple bi-fractal model is already sufficient for modelling apparently multifractal data [100]. For bi-fractal records the Renyi exponents $\tau(q)$ are characterised by two distinct slopes α_1 and α_2 ,

$$\tau(q) = \begin{cases} q\alpha_1 - 1 & q \leq q_\times \\ q\alpha_2 + q_\times(\alpha_1 - \alpha_2) - 1 & q > q_\times \end{cases} \quad (43)$$

or

$$\tau(q) = \begin{cases} q\alpha_1 + q_\times(\alpha_2 - \alpha_1) - 1 & q \leq q_\times \\ q\alpha_2 - 1 & q > q_\times \end{cases} . \quad (44)$$

If this behaviour is translated into the $h(q)$ picture using Eq. (29), we obtain that $h(q)$ exhibits a plateau from $q = -\infty$ up to a certain q_\times and decays hyperbolically for $q > q_\times$,

$$h(q) = \begin{cases} \alpha_1 & q \leq q_\times \\ q_\times(\alpha_1 - \alpha_2)\frac{1}{q} + \alpha_2 & q > q_\times \end{cases} , \quad (45)$$

or vice versa,

$$h(q) = \begin{cases} q_\times(\alpha_2 - \alpha_1)\frac{1}{q} + \alpha_1 & q \leq q_\times \\ \alpha_2 & q > q_\times \end{cases} . \quad (46)$$

Both versions of this bi-fractal model require three parameters. The multifractal spectrum is degenerated to two single points, thus its width can be defined as $\Delta\alpha = \alpha_1 - \alpha_2$.

9 Future Directions

The most straightforward future direction is to analyse more types of time series from other complex systems than those listed in Chapter 2 to check for the presence of fractal scaling and in particular long-term correlations. Such applications may include (i) data that are not recorded as function of time but as function of another parameter and (ii) higher dimensional data. In particular, the inter-relationship between fractal time series and spatially fractal structures can be studied. Studies of *fields* with fractal scaling in time and space have already been performed in Geophysics. In some cases studying new types of data will require dealing with more difficult types of non-stationarities and transient behaviour, making further development of the methods necessary. In many studies, detrending methods have not been applied yet. However, discovering fractal scaling in more and more systems cannot be an aim on its own.

Up to now, the reasons for observed fractal or multifractal scaling are not clear in most applications. It is thus highly desirable to study causes for fractal and multifractal correlations in time series, which is a difficult task, of course. One approach might be based on modelling and comparing the fractal aspects of real and modelled time series by applying the methods described in this article. The fractal or multifractal characterisation can thus be helpful in improving the models. For many applications, practically usable models which display fractal or transient fractal scaling still have to be developed. One example for a model explaining fractal scaling might be a precipitation, storage, and runoff model, in which the fractal scaling of runoff time series could be explained by fractional integration of rainfall in soil, groundwater reservoirs, or river networks characterised by a fractal structure. Also studies regarding the inter-relation between fractal scaling and complex networks, representing the structure of a complex system, are desirable. This way one could gain an interpretation of the causes for fractal behaviour.

Another direction of future research is regarding the linear and especially non-linear inter-relations between several time series. There is great need for improved methods characterising cross-correlations and similar statistical inter-relations between several non-stationary time series. Most methods available so far are reserved to stationary data, which is, however, hardly found in natural recordings. See [101] for a very recent approach analysing fractal cross-correlations in non-stationary data. An even more ambitious aim is the (time-dependent) characterisation of a larger network of signals. In such a network, the signals themselves would represent the nodes, while the (possibly directed) inter-relations between each pair represent the links

(or bonds) between the nodes. The properties of both, nodes and links can vary with time or change abruptly, when the represented complex system goes through a phase transition.

Finally, more work will have to be invested in studying the practical consequences of fractal scaling in time series. Studies should particularly focus on predictions of future values and behaviour of time series and whole complex systems. This is very relevant, not only in hydrology and climate research, where a clear distinguishing of trends and natural fluctuations is crucial, but also for predicting dangerous medical events on-line in patients based on the continuous recording of time series.

Acknowledgement: We thank Ronny Bartsch, Amir Bashan, Mikhail Bogachev, Armin Bunde, Jan Eichner, Shlomo Havlin, Diego Rybski, Aicko Schumann, and Stephan Zschiegner for helpful discussions. This work has been supported by the Deutsche Forschungsgemeinschaft (grant KA 1676/3) and the European Union (STREP project DAPHNet, grant 018474-2).

10 Bibliography

References

- [1] B.B. Mandelbrot, J.W. van Ness, *Fractional Brownian motions, fractional noises and applications*, SIAM Review **10**, 422 (1968).
- [2] B.B. Mandelbrot, J.R. Wallis, *Some long-run properties of geophysical records*, Water Resour. Res. **5**, 321-340 (1969).
- [3] Benoit B. Mandelbrot, *Multifractals and 1/f noise: wild self-affinity in physics* (Springer, Berlin 1999).
- [4] H.E. Hurst, *Long-term storage capacity of reservoirs*, Transactions of the American Society of Civil Engineering **116**, 770 (1951).
- [5] H.E. Hurst, R.P. Black, Y.M. Simaika, *Long-term storage: an experimental study* (Constable and Co., Ltd, London, 1965).
- [6] J. Feder, *Fractals* (Plenum Press, New York, 1988).
- [7] M.F. Barnsley, *Fractals everywhere* (Academic Press, 1993).
- [8] *Fractals in science*, edited by A. Bunde, S. Havlin (Springer, Berlin 1994).

- [9] P.E.T. Jorgensen, *Analysis and probability: wavelets, signals, fractals* (Springer, Berlin 2000).
- [10] *The science of disasters – climate disruptions, heart attacks, and market crashes*, edited by A. Bunde, J. Kropp, H.-J. Schellnhuber (Springer, Berlin 2002).
- [11] H. Kantz, T. Schreiber, *Nonlinear time series analysis* (Cambridge University Press, 2003).
- [12] H.-O. Peitgen, H. Jürgens, D. Saupe, *Chaos and fractals* (Springer, Berlin, 2004)
- [13] D. Sornette, *Critical phenomena in natural sciences* (Springer, Berlin, 2004).
- [14] C.-K. Peng, J. Mietus, J.M. Hausdorff, S. Havlin, H.E. Stanley, A.L. Goldberger, *Long-range anti-correlations and non-Gaussian behaviour of the heartbeat*, Phys. Rev. Lett. **70**, 1343 (1993).
- [15] A. Bunde, S. Havlin, J. W. Kantelhardt, T. Penzel, J.-H. Peter, K. Voigt, *Correlated and uncorrelated regions in heart-rate fluctuations during sleep*, Phys. Rev. Lett. **85**, 3736 (2000).
- [16] D. Vyushin, I. Zhidkov, S. Havlin, A. Bunde, S. Brenner, *Volcanic forcing improves atmosphere-ocean coupled general circulation model scaling performance*, Geophys. Res. Lett. **31**, L10206 (2004).
- [17] E. Koscielny-Bunde, A. Bunde, S. Havlin, H.E. Roman, Y. Goldreich, H.J. Schellnhuber, *Indication of a universal persistence law governing atmospheric variability*, Phys. Rev. Lett. **81**, 729 (1998).
- [18] G.E.P. Box, G.M. Jenkins, G.C. Reinsel, *Time-series Analysis* (Prentice Hall, New Jersey 1994).
- [19] C. Chatfield, *The analysis of time series. An introduction* (Taylor & Francis Ltd., 2003).
- [20] D.T. Schmitt, M. Schulz, *Analyzing memory effects of complex systems from time series*, Phys. Rev. E **73**, 056204 (2006).
- [21] M.S. Taqqu, V. Teverovsky, W. Willinger, *Estimators for long-range dependence: An empirical study*, Fractals **3**, 785 (1995).

- [22] D. Delignieres, S. Ramdania, L. Lemoine, K. Torrea, M. Fortesb, G. Ninot, *Fractal analyses for 'short' time series: A re-assessment of classical methods*, J. Math. Psychol. **50**, 525 (2006).
- [23] J. Mielniczuk, P. Wojdylo, *Estimation of Hurst exponent revisited*, Comp. Stat. Data. Anal. **51**, 4510 (2007).
- [24] G.A. Hunt, *Random Fourier transforms*, Trans. Amer. Math. Soc. **71**, 38 (1951).
- [25] G. Rangarajan, M. Ding, *Integrated approach to the assessment of long range correlation in time series data*, Phys. Rev. E **61**, 4991 (2000).
- [26] C.-K. Peng, S.V. Buldyrev, A.L. Goldberger, S. Havlin, F. Sciortino, M. Simons, H.E. Stanley, *Long-range correlations in nucleotide sequences*, Nature **356**, 168 (1992).
- [27] P. Goupillaud, A. Grossmann, J. Morlet, *Cycle-octave and related transforms in seismic signal analysis*, Geoexploration **23**, **85** (1984).
- [28] I. Daubechies, *Orthogonal bases of compactly supported wavelets*, Commun. Pure Appl. Math. **41**, 909 (1988).
- [29] J. W. Kantelhardt, H. E. Roman, M. Greiner, *Discrete wavelet approach to multifractality*, Physica A **220**, 219 (1995).
- [30] C.-K. Peng, S.V. Buldyrev, S. Havlin, M. Simons, H.E. Stanley, A.L. Goldberger, *Mosaic organization of DNA nucleotides*, Phys. Rev. E **49**, 1685 (1994).
- [31] Y. Ashkenazy, P. Ch. Ivanov, S. Havlin, C.-K. Peng, A. L. Goldberger, H. E. Stanley, *Magnitude and sign correlations in heartbeat fluctuations*, Phys. Rev. Lett. **86**, 1900 (2001).
- [32] J.W. Kantelhardt, S.A. Zschiegner, A. Bunde, S. Havlin, E. Koscielny-Bunde, H.E. Stanley, *Multifractal detrended fluctuation analysis of non-stationary time series*, Physica A **316**, 87 (2002).
- [33] G.-F. Gu, W.-X. Zhou, *Detrended fluctuation analysis for fractals and multifractals in higher dimensions*, Phys. Rev. E **74**, 061104 (2006)
- [34] J.W. Kantelhardt, E. Koscielny-Bunde, H.H.A. Rego, S. Havlin, A. Bunde, *Detecting long-range correlations with detrended fluctuation analysis*, Physica A **295**, 441 (2001).

- [35] K. Hu, P.Ch. Ivanov, Z. Chen, P. Carpena, H.E. Stanley, *Effect of trends on detrended fluctuation analysis*, Phys. Rev. E **64**, 011114 (2001).
- [36] Z. Chen, P.Ch. Ivanov, K. Hu, H.E. Stanley, *Effect of non-stationarities on detrended fluctuation analysis*, Phys. Rev. E **65**, 041107 (2002).
- [37] Z. Chen, K. Hu, P. Carpena, P. Bernaola-Galvan, H.E. Stanley, P.Ch. Ivanov, *Effect of nonlinear filters on detrended fluctuation analysis*, Phys. Rev. E **71**, 011104 (2005).
- [38] P. Grau-Carles, *Bootstrap testing for detrended fluctuation analysis*, Physics A **360**, 89 (2006).
- [39] R. Nagarajan, *Effect of coarse-graining on detrended fluctuation analysis*, Physica A **363**, 226 (2006).
- [40] C. Heneghan, G. McDarby, *Establishing the relation between detrended fluctuation analysis and power spectral density analysis for stochastic processes*, Phys. Rev. E **62**, 6103 (2000).
- [41] R. Weron, *Estimating long-range dependence: finite sample properties and confidence intervals*, Physica A **312**, 285 (2002).
- [42] A. Bashan, R. Bartsch, J.W. Kantelhardt, S. Havlin, *Comparison of detrending methods for fluctuation analysis*, Physica A (in press, 2008).
- [43] S. Bahar, J.W. Kantelhardt, A. Neiman, H.H.A. Rego, D.F. Russell, L. Wilkens, A. Bunde, F. Moss, *Long range temporal anti-correlations in paddlefish electro-receptors*, Europhys. Lett. **56**, 454 (2001).
- [44] R. Bartsch, T. Henning, A. Heinen, S. Heinrichs, P. Maass, *Statistical analysis of fluctuations in the ECG morphology*, Physica A **354**, 415 (2005).
- [45] M.S. Santhanam, J.N. Bandyopadhyay, and D. Angom, *Quantum spectrum as a time series: fluctuation measures*, Phys. Rev. E **73**, 015201 (2006).
- [46] Y. Ashkenazy, S. Havlin, P.Ch. Ivanov, C.-K. Peng, V. Schulte-Frohlinde, H.E. Stanley, *Magnitude and sign scaling in power-law correlated time series*, Physica A **323**, 19 (2003).
- [47] T. Kalisky, Y. Ashkenazy, S. Havlin, *Volatility of linear and nonlinear time series*, Phys. Rev. E **72**, 011913 (2005).

- [48] R.N. Mantegna, H.E. Stanley, *An introduction to econophysics – correlations and complexity in finance* (Cambridge Univ. Press, 2000).
- [49] J.-P. Bouchaud, M. Potters, *Theory of financial risks: from statistical physics to risk management* (Cambridge Univ. Press, 2003).
- [50] E. Alessio, A. Carbone, G. Castelli, V. Frappietro, *Second-order moving average and scaling of stochastic time series*, *Europ. Phys. J. B* **27**, 197 (2002).
- [51] A. Carbone, G. Castelli, H.E. Stanley, *Analysis of clusters formed by the moving average of a long-range correlated time series*, *Phys. Rev. E* **69**, 026105 (2004).
- [52] A. Carbone, G. Castelli, H.E. Stanley, *Time-dependent Hurst exponent in financial time series*, *Physica A* **344**, 267 (2004).
- [53] J. Alvarez-Ramirez, E. Rodriguez, J.C. Echeverría, *Detrending fluctuation analysis based on moving average filtering*, *Physica A* **354**, 199 (2005).
- [54] K. Kiyono, Z.R. Struzik, N. Aoyagi, F. Togo, Y. Yamamoto, *Phase transition in a healthy human heart rate*, *Phys. Rev. Lett.* **95**, 058101 (2005).
- [55] M. Staudacher, S. Telser, A. Amann, H. Hinterhuber, M. Ritsch-Marte, *A new method for change-point detection developed for on-line analysis of the heart beat variability during sleep*, *Physica A* **349**, 582 (2005).
- [56] S. Telser, M. Staudacher, B. Hennig, Y. Ploner, A. Amann, H. Hinterhuber, M. Ritsch-Marte, *Temporally resolved fluctuation analysis of sleep-ECG*, *J. Biol. Phys.* (Preprint, 2007).
- [57] C.V. Chianca, A. Ticona, T.J.P. Penna, *Fourier-detrended fluctuation analysis*, *Physica A* **357**, 447 (2005).
- [58] I.M. János, R. Müller, *Empirical mode decomposition and correlation properties of long daily ozone records*, *Phys. Rev. E* **71**, 056126 (2005).
- [59] R. Nagarajan, R.G. Kavasseri, *Minimizing the effect of trends on detrended fluctuation analysis of long-range correlated noise*, *Physica A* **354**, 182 (2005).
- [60] R. Nagarajan, *Reliable scaling exponent estimation of long-range correlated noise in the presence of random spikes*, *Physica A* **366**, 1 (2006).

- [61] E. Rodriguez, J.C. Echeverria, J. Alvarez-Ramirez, *Detrending fluctuation analysis based on high-pass filtering*, Physica A **375**, 699 (2007).
- [62] D. Grech and Z. Mazur, *Statistical properties of old and new techniques in detrended analysis of time series*, Acta Phys. Pol. B **36**, 2403 (2005).
- [63] L. Xu, P.Ch. Ivanov, K.Hu, Z. Chen, A. Carbone, and H.E. Stanley, *Quantifying signals with power-law correlations: a comparative study of detrended fluctuation analysis and detrended moving average techniques*, Phys. Rev. E **71**, 051101 (2005).
- [64] A.-L. Barabási, T. Vicsek, *Multifractality of self-affine fractals*, Phys. Rev. A **44**, 2730 (1991).
- [65] E. Bacry, J. Delour, J.F. Muzy, *Multifractal random walk*, Phys. Rev. E **64**, 026103 (2001).
- [66] J.F. Muzy, E. Bacry, A. Arneodo, *Wavelets and multifractal formalism for singular signals: Application to turbulence data*, Phys. Rev. Lett. **67**, 3515 (1991).
- [67] J.F. Muzy, E. Bacry, A. Arneodo, *The multifractal formalism revisited with wavelets*, Int. J. Bifurcat. Chaos **4**, 245 (1994).
- [68] A. Arneodo, E. Bacry, P.V. Graves, J.F. Muzy, *Characterizing long-range correlations in DNA sequences from wavelet analysis*, Phys. Rev. Lett. **74**, 3293 (1995).
- [69] A. Arneodo, S. Manneville, J.F. Muzy, *Towards log-normal statistics in high Reynolds number turbulence*, Eur. Phys. J. B **1**, 129 (1998).
- [70] A. Arneodo, B. Audit, N. Decoster, J.F. Muzy, C. Vaillant, *Wavelet based multifractal formalism: applications to DNA sequences, satellite images of the cloud structure, and stock market data*, in: *The science of disaster: climate disruptions, market crashes, and heart attacks*, edited by A. Bunde, J. Kropp, H.-J. Schellnhuber (Springer, Berlin, 2002).
- [71] J.W. Kantelhardt, D. Rybski, S.A. Zschiegner, P. Braun, E. Koscielny-Bunde, V. Livina, S. Havlin, A. Bunde, *Multifractality of river runoff and precipitation: comparison of fluctuation analysis and wavelet methods*, Physica A **330**, 240 (2003).
- [72] P. Oswiecimka, J. Kwapien, S. Drozd, *Wavelet versus detrended fluctuation analysis of multifractal structures*, Phys. Rev. E **74**, 016103 (2006).

- [73] P.Ch. Ivanov, L.A.N. Amaral, A.L. Goldberger, S. Havlin, M.G. Rosenblum, Z.R. Struzik, H.E. Stanley, *Multifractality in human heartbeat dynamics*, Nature **399**, 461 (1999).
- [74] L.A.N. Amaral, P.Ch. Ivanov, N. Aoyagi, I. Hidaka, S. Tomono, A.L. Goldberger, H.E. Stanley, Y. Yamamoto, *Behavioral-independence features of complex heartbeat dynamics*, Phys. Rev. Lett. **86**, 6026 (2001).
- [75] M. Bogachev, A.Y. Schumann, J. W. Kantelhardt, in preparation (2008).
- [76] A. Bunde, J.F. Eichner, J.W. Kantelhardt, S. Havlin, *Long-term memory: A natural mechanism for the clustering of extreme events and anomalous residual times in climate records*, Phys. Rev. Lett. **94**, 048701 (2005).
- [77] A. Bunde, J.F. Eichner, J.W. Kantelhardt, S. Havlin, *The effect of long-term correlations on the return periods of rare events*, Physica A **330**, 1 (2003).
- [78] E.G. Altmann, H. Kantz, *Recurrence time analysis, long-term correlations, and extreme events*, Phys. Rev. E **71**, 056106 (2005).
- [79] J.F. Eichner, J.W. Kantelhardt, A. Bunde, S. Havlin, *Statistics of return intervals in long-term correlated records*, Phys. Rev. E **75**, 011128 (2007).
- [80] J.F. Eichner, J.W. Kantelhardt, A. Bunde, S. Havlin, *Extreme value statistics in records with long-term persistence*, Phys. Rev. E **73**, 016130 (2006).
- [81] M.I. Bogachev, J.F. Eichner, A. Bunde, *Effect of nonlinear correlations on the statistics of return intervals in multifractal data sets*, Phys. Rev. Lett. **99**, 240601 (2007).
- [82] H. v. Storch, F.W. Zwiers, *Statistical analysis in climate research* (Cambridge Univ. Press, 2001).
- [83] G.F. Newell, M. Rosenblatt, Ann. Math. Statist. **33**, 1306 (1962).
- [84] D. Sornette, L. Knopoff, *The paradox of the expected time until the next earthquake*, Bull. Seism. Soc. Am. **87**, 789 (1997).
- [85] R.A. Fisher, L.H.C. Tippett, *Limiting forms of the frequency distribution of the largest or smallest member of a sample*, Proc. Camb. Phil. Soc. **24**, 180 (1928).

- [86] E.J. Gumbel, *Statistics of extremes* (Columbia University Press, New York, 1958).
- [87] J. Galambos, *The asymptotic theory of extreme order statistics*, (John Wiley and Sons, New York, 1978).
- [88] M.R. Leadbetter, G. Lindgren, H. Rootzen, *Extremes and related properties of random sequences and processes* (Springer, New York, 1983).
- [89] *Extreme value theory and applications*, edited by J. Galambos, J. Lechner, E. Simin (Kluwer, Dordrecht, 1994).
- [90] V. te Chow, *Handbook of applied hydrology* (McGraw-Hill Book Company, New York, 1964).
- [91] A.J. Raudkivi, *Hydrology* (Pergamon Press, Oxford, 1979).
- [92] P.F. Rasmussen, N. Gautam, *Alternative PWM-estimators of the Gumbel distribution*, J. Hydrol. **280**, 265 (2003).
- [93] B.B. Mandelbrot, *A fast fractional Gaussian noise generator*, Water Resour. Res. **7**, 543 (1971).
- [94] R.F. Voss, in: *Fundamental algorithms in computer graphics* edited by R.A. Earnshaw (Springer, Berlin, 1985).
- [95] H.A. Makse, S. Havlin, M. Schwartz, H.E. Stanley, *Method for generating long-range correlations for large systems*, Phys. Rev. E **53**, 5445 (1996).
- [96] I. Rodriguez-Iturbe, A. Rinaldo, *Fractal river basins – change and self-organization* (Cambridge Univ. Press, 1997).
- [97] T. Schreiber, A. Schmitz, *Improved surrogate data for nonlinearity tests*, Phys. Rev. Lett. **77**, 635 (1996).
- [98] T. Schreiber, A. Schmitz, *Surrogate time series*, Physica D **142**, 346 (2000).
- [99] E. Koscielny-Bunde, J.W. Kantelhardt, P. Braun, A. Bunde und S. Havlin, *Long-term persistence and multifractality of river runoff records*, J. Hydrol. **322**, 120 (2006).

- [100] J.W. Kantelhardt, E. Koscielny-Bunde, D. Rybski, P. Braun, A. Bunde, S. Havlin, *Long-term persistence and multifractality of precipitation and river runoff records*, J. Geophys. Res. (Atmosph.) **111**, D01106 (2006).
- [101] B. Podobnik, H.E. Stanley, *Detrended cross-correlation analysis: a new method for analyzing two nonstationary time series*, Phys. Rev. Lett. **100**, 084102 (2008).

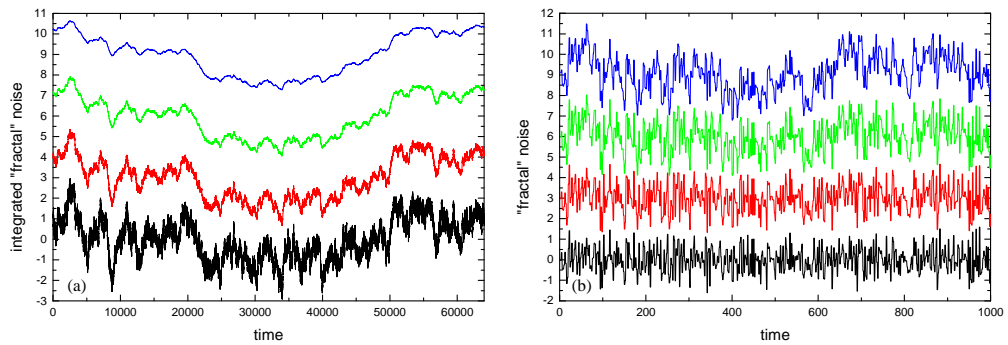


Figure 1: (a) Examples of self-affine series x_i characterized by different Hurst exponents $H = 0.9, 0.7, 0.5, 0.3$ (from top to bottom). The data has been generated by Fourier filtering (see Section 8.1) using the same seed for the random number generator. (b) Differentiated series Δx_i of the data from (a); the Δx_i are characterized by positive long-term correlations (persistence) with $\gamma = 0.2$ and 0.6 (top curve and second curve), uncorrelated behaviour (third curve), and anti-correlations (bottom curve), respectively.

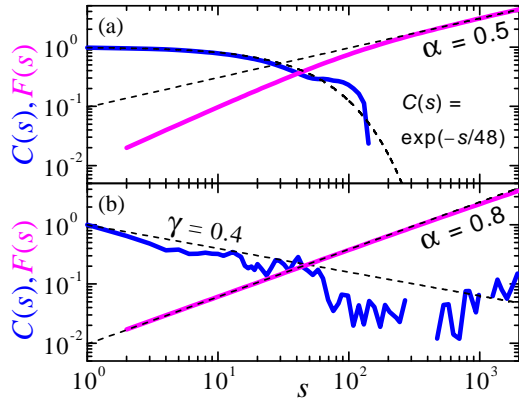


Figure 2: Comparison of the autocorrelation functions $C(s)$ (decreasing functions) and fluctuation functions $F_2(s)$ (increasing functions) for short-term correlated data (top) and long-term correlated data ($\gamma = 0.4$, bottom). The asymptotic slope $H \approx \alpha = 0.5$ of $F_2(s)$ clearly indicates the absence of long-term correlations, while $H \approx \alpha = 1 - \gamma/2 > 0.5$ indicates the presence long-term correlations. The difference is much harder to observe in $C(s)$, where there are more statistical fluctuations and even negative values (e.g., above $s = 150$ in (a) and between $s = 300$ and 400 in (b), not shown). The data have been generated by an AR process (Eq. (4)) and Fourier filtering (Section 8.1) for (a) and (b), respectively. The dashed lines indicate the theoretical curves.

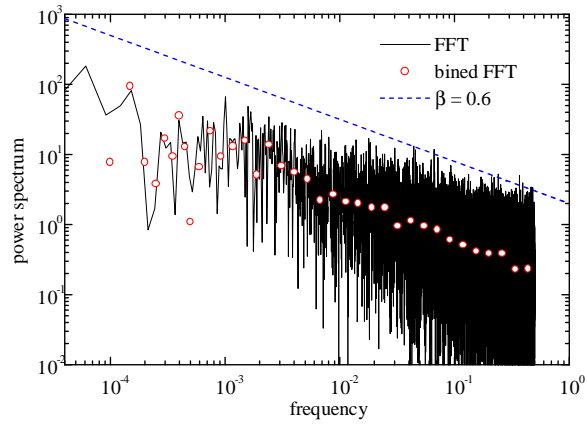


Figure 3: Spectral analysis of a fractal time series characterized by long-term correlations with $\gamma = 0.4$ ($\beta = 0.6$). The expected scaling behaviour (dashed line indicating the slope $-\beta$) is observed only after binning of the spectrum (circles). The data has been generated by Fourier filtering (see Section 8.1).

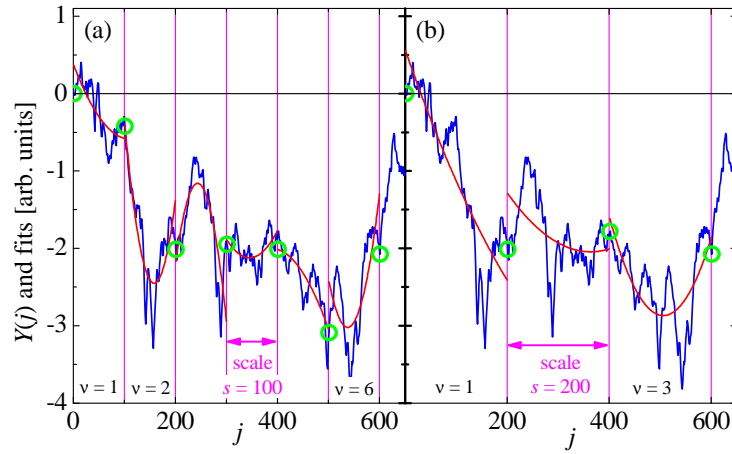


Figure 4: Illustration of the Fluctuation Analysis (FA) and the Detrended Fluctuation Analysis (DFA). For two segment durations (time scales) $s = 100$ (a) and 200 (b), the profiles $Y(j)$ (blue lines; defined in Eq. (10)), the values $Y(vs)$ used for the FA in Eq. (11) (green circles), and least square quadratic fits to the profiles used in DFA (red lines) are shown.

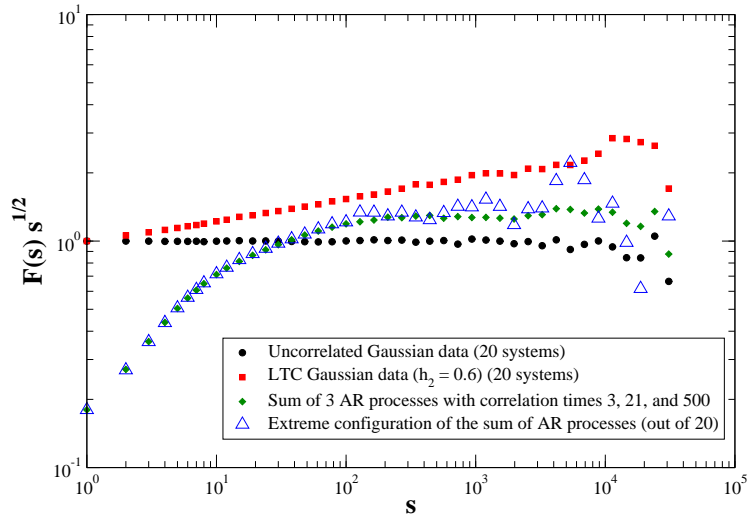


Figure 5: Application of discrete wavelet transform (WT) analysis on uncorrelated data (black circles), long-term correlated data ($\gamma = 0.8$, $\alpha = 0.6$, red squares), and short-term correlated data (summation of three AR processes, green diamonds). Averages of $F_2(s)$ averaged over 20 series with $N = 2^{16}$ points and divided by $s^{1/2}$ are shown, so that a horizontal line corresponds to uncorrelated behaviour. The blue open triangles show the result for one selected extreme configuration, where it is hard to decide about the existence of long-term correlations (figure prepared by Mikhail Bogachev).

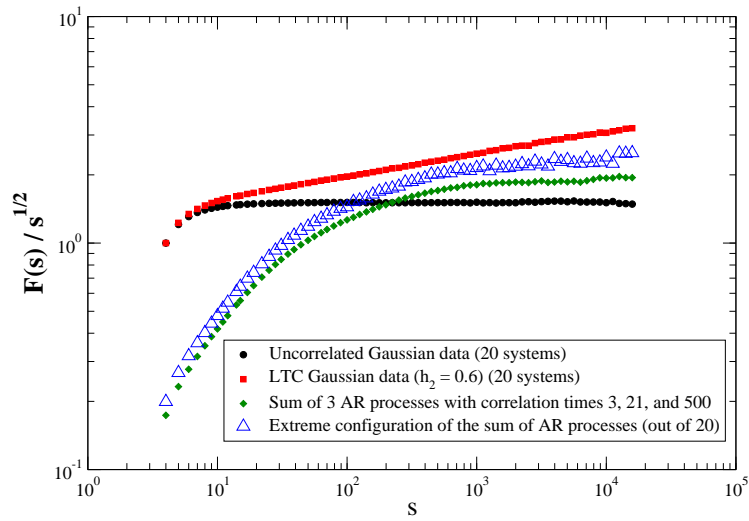


Figure 6: Application of Detrended Fluctuation Analysis (DFA) on the data already studied in Fig. 5 (figure by Mikhail Bogachev).

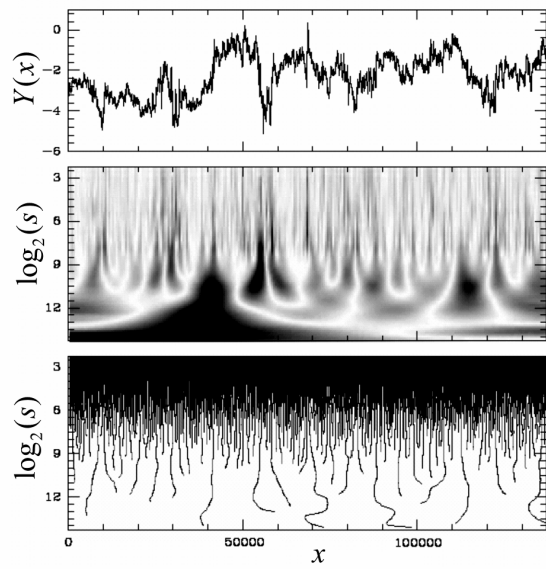


Figure 7: Example of the Wavelet Transform Modulus Maxima (WTMM) method, showing the original data (top), its continuous wavelet transform (grey scale coded amplitude of wavelet coefficients, middle), and the extracted maxima lines (bottom) (figure taken from [67]).

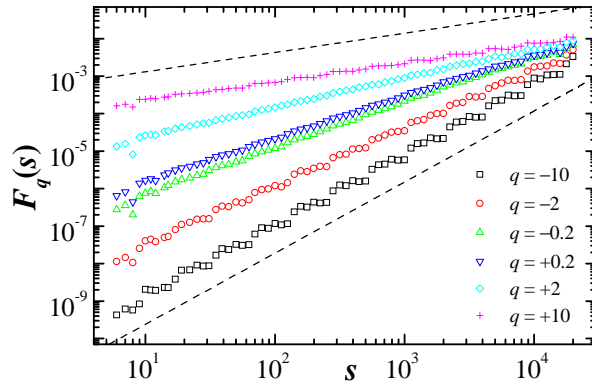


Figure 8: Multifractal Detrended Fluctuation Analysis (MF-DFA) of data from the binomial multifractal model (see Section 8.3) with $a = 0.75$. $F_q(s)$ is plotted versus s for the q values given in the legend; the slopes of the curves correspond to the values of $h(q)$. The dashed lines have the slopes of the theoretical slopes $h(\pm\infty)$ from Eq. (42). 100 configurations have been averaged.

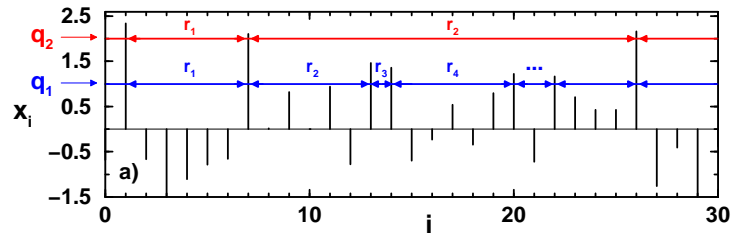


Figure 9: Illustration for the definition of return intervals r_q between extreme events above two quantiles (thresholds) q_1 and q_2 (figure by Jan Eichner).

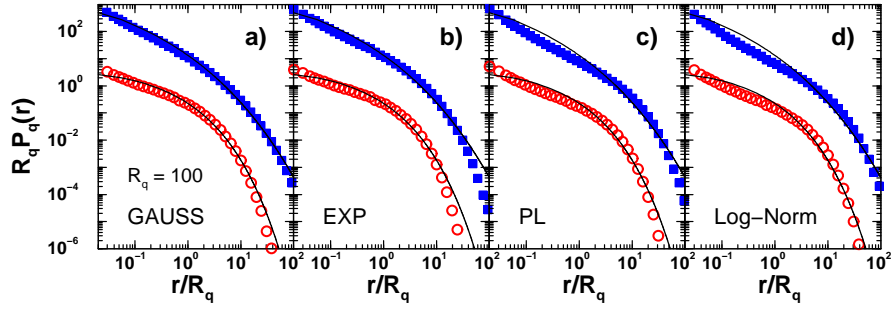


Figure 10: Normalized rescaled distribution density functions $R_q P_q(r)$ of r values with $R_q = 100$ as a function of r/R_q for long-term correlated data with $\gamma = 0.4$ (open symbols) and $\gamma = 0.2$ (filled symbols; we multiplied the data for the filled symbols by a factor 100 to avoid overlapping curves). In (a) the original data was Gaussian distributed, in (b) exponentially distributed, in (c) power-law distributed with power -5.5 , and in (d) log-normally distributed. All four figures follow quite well stretched exponential curves (solid lines) over several decades. For small r/R_q values a power-law regime seems to dominate, while on large scales deviations from the stretched exponential behaviour are due to finite-size effects (figure by Jan Eichner).

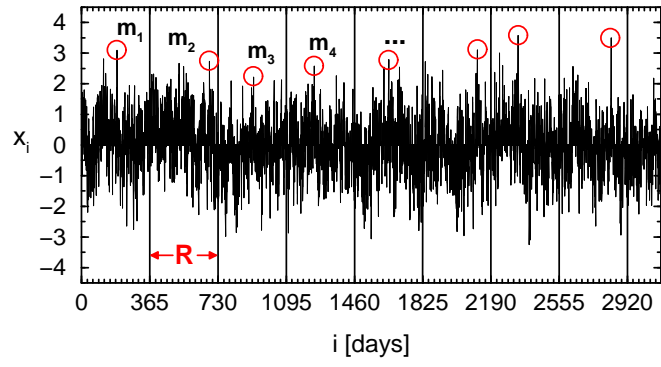


Figure 11: Illustration for the definition of maxima m_R within periods of $R = 365$ values (figure by Jan Eichner).